AFOSR-TR. 89-0089

Annual Technical Report #1
November 1, 1987 - November 1, 1988

ANALYSIS OF FLOW-, THERMAL- AND STRUCTURAL-INTERACTION OF HYPERSONIC STRUCTURES SUBJECTED TO SEVERE AERODYNAMIC HEATING

Contract No. F49620-C-0001

Air Force Office of Scientific Research
Building 410
Bolling AFB, DC 20332-6448

TR-88-12

THE COMPUTATIONAL MECHANICS CO., INC.
3701 North Lamar, Suite 201
Austin, Texas 78705
(512) 467-0618

THE COMPUTATIONAL MECHANICS COMPANY, INC.

89   2   15   168

REPORT DOCUMENTATION PAGE

Form Approved
OMB No. 0704-0188

1a. REPORT SECURITY CLASSIFICATION	1b. RESTRICTIVE MARKINGS
Unclassified	None

2a. SECURITY CLASSIFICATION AUTHORITY	3. DISTRIBUTION / AVAILABILITY OF REPORT
2b. DECLASSIFICATION / DOWNGRADING SCHEDULE	Approved for public release, distribution unlimited

4. PERFORMING ORGANIZATION REPORT NUMBER(S)	5. MONITORING ORGANIZATION REPORT NUMBER(S)
TR-88-12	AFOSR-TR· 89-0089

6a. NAME OF PERFORMING ORGANIZATION	6b. OFFICE SYMBOL (If applicable)	7a. NAME OF MONITORING ORGANIZATION
Computaional Mechanics Company, Inc.		AFOSR

6c. ADDRESS (City, State, and ZIP Code)	7b. ADDRESS (City, State, and ZIP Code)
3701 North Lamar, Suite 201 Austin TX 78705	Same as 8C.

8a. NAME OF FUNDING / SPONSORING ORGANIZATION USAF, AFSC Air Force Office of Scientific Research	8b. OFFICE SYMBOL (If applicable) NA	9. PROCUREMENT INSTRUMENT IDENTIFICATION NUMBER F49620-88-C-0001

8c. ADDRESS (City, State, and ZIP Code)	10. SOURCE OF FUNDING NUMBERS			
Bolling Air Force Base DC 20332 Bldg 410	PROGRAM ELEMENT NO. 61102F	PROJECT NO. 2302	TASK NO. B1	WORK UNIT ACCESSION N

11. TITLE (Include Security Classification)
"Analysis of Flow-, Thermal-, and Structural-Interaction of Hypersonic Structures Subjected to Severe Aerodynamic Heating" (U)

12. PERSONAL AUTHOR(S)
J. T. Oden / E. A. Thornton

13a. TYPE OF REPORT	13b. TIME COVERED	14. DATE OF REPORT (Year, Month, Day)	15. PAGE COUNT
Annual Technical	FROM 11-1-87 TO 11-1-88	November 30, 1988	51

16. SUPPLEMENTARY NOTATION

17.	COSATI CODES		18. SUBJECT TERMS (Continue on reverse if necessary and identify by block number)
FIELD	GROUP	SUB-GROUP	Flow-, thermal-, and structural-interaction, hypersonic flow, aerodynamic heating, viscous flow, unified viscoplastic theories, convective cooling,

19. ABSTRACT (Continue on reverse if necessary and identify by block number)

This first annual report presents progress in the modelling of hypersonic fluid-thermal-structural interaction. In this phase of the effort, the basic mechanisms of heat transfer and fluid-structure interaction were identified. Mathematical models for heat transfer, structural deformation and fluid flow analysis were formulated. New unified viscoplastic theories were adapted for the modelling of complex visco-elasto-plastic structural deformation, with temperature-dependent material properties. A general procedure for the analysis of fluid-thermal-structure interaction was formulated, and relevant finite element codes were developed. These problems were applied in the solution of representative examples of thermo-structural analysis of structures subject to aerodynamic heating. These programs of adaptive finite element analysis of viscous flow were also developed and validated on selected examples. Finally, directions for further research in the project were developed.

20. DISTRIBUTION / AVAILABILITY OF ABSTRACT	21. ABSTRACT SECURITY CLASSIFICATION
☒ UNCLASSIFIED/UNLIMITED ☐ SAME AS RPT ☒ DTIC USERS	Unclassified

22a. NAME OF RESPONSIBLE INDIVIDUAL	22b. TELEPHONE (Include Area Code)	22c. OFFICE SYMBOL
Dr. Anthony K. Amos	(202) 767-4937	N

DD Form 1473, JUN 86   Previous editions are obsolete.   SECURITY CLASSIFICATION OF THIS PAGE

Annual Technical Report #1
November 1, 1987 - November 1, 1988

ANALYSIS OF FLOW-,
THERMAL- AND STRUCTURAL-INTERACTION
OF
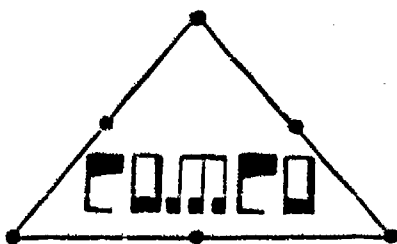# HYPERSONIC STRUCTURES
SUBJECTED TO SEVERE AERODYNAMIC
HEATING

Contract No. F49620-C-0001

Air Force Office of Scientific Research
Building 410
Bolling AFB, DC 20332-6448

TR-88-12

THE COMPUTATIONAL MECHANICS CO., INC.
3701 North Lamar, Suite 201
Austin, Texas 78705
(512) 467-0618

THE COMPUTATIONAL MECHANICS COMPANY, INC.

Contents

1 Introduction

The commitment to develop the National Aerospace Plane (NASP) has generated resurgent interest in the technology required to develop structures for hypersonic flight. Such structures will be exposed to aerodynamic heating of unprecedented magnitudes. NASA estimated surface temperatures for NASP are shown in Fig. 1. As the vehicle accelerates or decelerates at hypersonic speeds in the earth's atmosphere, shock waves will sweep across the vehicle and interact with local shocks and boundary layers. These interactions introduce severe local pressures and heating rates. A recent experimental study (ref.1) of interacting shock waves on a cylindrical leading edge shows heating rates ten times undisturbed levels.

Leading edges of engine structures present a signficant design problem because of intense local heating and pressures. Analysis of the flow, thermal and structural behavior present serious computational challenges to analysts because of the inherent nonlinearities in all aspects of the multi-disciplinary problems. Some of the critical computational issues are identified in ref. 2. Critical issues include the difficulties involved in: (1) analyzing the viscous, compressible flow and predicting the high local aerodynamic heating, (2) modeling and analyzing multi-mode unsteady heat transfer in a high temperature convectively-cooled structure, and (3) simulating the transient, nonlinear thermal-structural response for rapid temperature changes. Preliminary structural analysis of an impingement cooled leading edge (ref.3) showed high local plasticity that seriously degraded the structure's load carrying capacity at elevated temperatures. A recent thermostructural analysis with experimental verification (ref.4) of cowl lip designs confirmed that significant inelastic effects occur. In the experimental study, two specimens failed due to burn-through because of intense local heating or because of loss of cooling.

This research contract addresses fundamental issues relevant to the development of hypersonic structures subject to severe thermal loads. The specific objectives of the current research include:

1. An investigation of the processes and theories for energy transfer between high temperature steady hypersonic flows and deformable aerodynamic structures.

1

2. Identification of mechanisms for heat transfer in hypersonic structures subjected to intense heating rates. Development of mathematical models for high temperature, inelastic response of structures considering the effects of time dependent, intense local heating and pressures.

3. Development of a unified finite element mesh refinement scheme for interdisciplinary problems including flow, thermal and structural response.

4. Studies of unsteady, transient problems of hypersonic flight involving structural interaction with the aerothermodynamics of the external flow.

2 Research Progress

The fluid-thermal-structural problems encountered on the NASP scramjet engine structure shown in Figure 2 are illustrative of the hypersonic interaction problems being considered. In the first year of this contract, work has focused on the physical phenomena, mathematical formulations, and computational methods needed to solve general problems of this type.

The flow-thermal-structure (F-T-S) interaction problem being considered is shown in Figure 3. Figure 3a shows a low temperature, undeformed elastic structure subjected to low-level, uniform aerodynamic heating. In this state, there is little F-T-S interaction. In contrast, Figure 3b shows a structure that is subjected to intense localized heating characteristic of shock interactions. There is a local, growing region of very high temperature plastically deforming material. As the plastic region grows, the surface deforms into the flow producing flow recirculation. The flow recirculation intensifies local heating, skin friction and surface pressure. As the heating increases, the temperature exceeds the melting temperature. Thereafter, a more complex interaction between the molten material and the external flow occurs. The F-T-S interaction including a molten region is not understood; the formulation and solution of this problem is a major goal of the research.

As steps toward achieving this goal, the following objectives have been accomplished:

1. A formulation of a coupled F-T-S interaction problem has been established assuming:

    (a) the unsteady heat transfer problem is described by conservation of energy neglecting mechanical coupling terms. This assumption is known to be reasonable for the materials, deformation rates and applied heat loads encountered in hypersonic structures. Nonlinear heat transfer due to temperature dependent material properties such as specific heat and thermal conductivity are included as well as surface radiation.

    (b) the structural problem is assumed to be quasi-static and viscoplastic. The quasi-static assumption means that inertia terms in the momentum equations may be neglected, and the structural problem can be formulated as a series of equilibrium problems due to time-varying temperature computed from the unsteady energy equation. The viscoplastic model assumes that strain rates are separated into elastic and plastic components. The plastic strain rate component is represented by constitutive equations known as unified viscoplastic

3

theories. Several unified theories exist with the common feature that strain rate dependent effects such as plastic flow, creep and stress relaxation are intrinsic to the formulation. The Bodner-Partom theory has been selected because of:

i. the availability of experimentally determined parameters for high temperature alloys, and

ii. the theory has been validated by experiments at elevated temperatures. The viscoplastic theory assumes that temperatures are less than 75 percent of the melting temperature.

(c) The flow problem is governed by the Navier-Stokes equations describing compressible flow. The principal assumption made is that the fluid is a calorically perfect gas. This assumption is legitimate for supersonic-hypersonic flows where the Mach number is less than, say, seven. Calorically perfect means that the gas specific heat is constant. For higher Mach numbers where the gas temperature is 2500K or higher the specific heat becomes temperature and pressure dependent, and the gas becomes chemically reactive.

2. Three finite element computer programs applicable to F-T-S interactions have been placed into operation.

(a) A family of finite element heat transfer programs capable of computing temperatures in high temperature structures is now operational. These programs model nonlinear conduction, radiation and forced convection heat transfer in convectively cooled hypersonic structures at elevated temperatures.

(b) a two-dimensional finite element thermo-viscoplastic program has been developed. The program is based on the Bodner-Partom unified viscoplastic constitutive model. Highly complex rate-dependent plasticity and creep phenomena at elevated temperatures can be simulated by the program.

The use of the Bodner-Partom theory in a finite element program has significant advantages, but the computational effort required to solve for the state variables in the constitutive equations is extensive. Sets of "stiff" ordinary differential equations must be integrated in time. Typically, these equations require very small steps, and hence large computer times are needed to capture the time-dependent phenomena. Time steps for the structural response are typically

about one-tenth of time steps required for the transient thermal analysis. This difference in time steps requires special techniques for interfacing the thermal and structural codes. An approach to interface the thermal program with the viscoplastic program has been developed and implemented. An adaptive time-step algorithm has been developed and implemented to give reliable, efficient solution of the stiff ordinary differential equations.

(c) A two-dimensional finite element viscous flow code has become operational. The program solves the conservation of mass, momentum and energy equations for compressible viscous flows. The conservation equations are solved using an explicit time–marching algorithm. An adaptive h refinement/derefinement scheme has been implemented. A "consistent" method for computing aerodynamic surface heating rates, skin friction (shearing stresses) and pressures has been developed and implemented. The capability of the viscous flow code to predict surface quantities is under evaluation.

3. Numerical computations have begun on a series of representative problems. Results of these computations are presented later in this report. The objectives of these computations are to:

(a) validate the codes, and

(b) study the basic processes that characterize F-T-S interactions.

4. A comprehensive literature search focused on the behavior and mathematical models of metallic materials at elevated temperatures has been accomplished. A significant number of relevant papers and reports have been acquired.

5. Visits to Southwest Research Institute and Texas A & M University have been made. Information on recent research in unified viscoplastic mathematical models was obtained as well as data describing material behavior at elevated temperatures. Implementation of these theories into finite element codes was discussed.

3 Thermal Analysis of Hypersonic Structures

Convectively cooled structures are strong candidates for use in hypersonic flight vehicles. For hypersonic flight, some leading edges and panels require active cooling systems to keep structural temperatures within acceptable ranges. The internal flow in the coolant passage has a predominant role in the thermal response of a hypersonic structure subject to external heating. A cross-section of a typical convectively cooled structure is shown in Figure 4. An aerodynamic skin and a coolant passage with internal heat exchanger protect the primary structure from the aerodynamic heating. The thin, typically metallic, aerodynamic skin transfers the energy of the aerodynamic heating to a low temperature coolant flow through the heat exchanger fins that connect the aerodynamic skin to the primary structure. In a typical engine structure, the coolant is cold hydrogen that later is used as the propulsion system fuel.

Heat transfer in the aerodynamic skin consists of conduction combined with surface radiation. Heat transfer between the aerodynamic skin, the heat exchanger surfaces and the primary structure is by conduction at the solid-fluid interface. The dominant mode of heat transfer in the coolant flow is forced convection.

The representation of the heat transfer in the coolant passage is the critical step in the heat transfer analysis. There are two basic representations that can be employed. The first, denoted here as the engineering model, is based upon a number of assumptions that greatly simplify the problem into a single energy equation with a specified mass flow rate. Detailed computation of the fluid velocity components and temperatures is not required. The second representation idealizes the coolant flow as a continuum model, and the partial differential equations describing conservation of mass, momentum and energy are solved simultaneously to obtain fluid velocity and temperature distributions. This latter model is the most accurate, but it is also considerably more expensive than the engineering model. As a first step towards understanding flow-thermal-structural interactions characteristic of hypersonic structures the engineering heat transfer models employed.

3.1 Engineering Model for Coolant Passages

The basic features of the engineering model can be developed from the idealization shown in Fig. 5. A segment of the coolant passage of width w is shown; for simplicity, only the upper one-half of the coolant passage with the aerodynamic skin is shown. The engineering formulation (ref.5) is based on the following assumptions:

6

1. The thermal energy state of the fluid is characterized by the fluid bulk temperature T_F which varies only in the flow direction, i.e. $T_F(x,t)$.

2. The flow is represented by the mass flow rate $\dot{m}$ in the coolant passage specified by $\dot{m} = \rho_F A_F V_F$ where ρ_F is the coolant density, A_F is the cross–sectional area of the coolant passage, and V_F is the coolant mean flow velocity.

3. A convection coefficient h is defined such that the heat flux $\dot{q}_F$ transferred between the structure and the coolant may be expressed as

$$\dot{q} = h(T_S - T_F)$$

where $T_S(x,t)$ denotes the structural temperature at the fluid–solid interface.

4. The convection coefficient h may be expressed as a function of the fluid bulk temperature alone by using analytical/empirical equations for the Nusselt number,

$$Nu = \frac{hD}{k_F}$$

where D is the hydraulic diameter of the coolant passage, and k_F is the thermal conductivity of the fluid coolant. The convection coefficient as well as the solid and fluid thermal parameters may, in general, be temperature dependent.

With these assumptions, energy balances on the aerodynamic skin and coolant give the governing conservation equations.

Fluid:
$$-\frac{\partial}{\partial x}\left(k_F A_F \frac{\partial T_F}{\partial x}\right) + \dot{m} c_F \frac{\partial T_F}{\partial x} - wh(T_S - T_F) + \rho_F c_F A_F \frac{\partial T_F}{\partial t} = 0 \qquad (3.1)$$

Solid:
$$-\frac{\partial}{\partial x}\left(k_S A_S \frac{\partial T_S}{\partial x}\right) + wh(T_S - T_F) + \sigma \epsilon T^4 + \rho_S c_S A_S \frac{\partial T_S}{\partial t} = \dot{q} \qquad (3.2)$$

where the subscripts F and S denote the fluid and solid, respectively. In these equations, c denotes specific heat, σ is the Stefan-Boltzmann constant, and ϵ is the surface emissivity. Because of the temperature dependence of the thermal parameters and the radiation term, Eqs. (3.1) and (3.2) constitute a nonlinear set of partial differential equations.

The heat exchanger fins are not included explicitly in this model. However, the heat transfer between the heat exchanger fins can approximately be taken into consideration though the use of an effective width w which represents the area over which the convective heat exchange occurs.

7

3.2 Finite Element Formulation

A typical finite element representing Eqs. (3.1) and (3.2) is characterized by fluid and fluid–solid interface nodes. The element shown in Fig. 6 has two fluid nodes (I and J), and two fluid–solid interface nodes. Within the element, the fluid and solid temperatures are express as

$$T_F = [N(x)]\{T_F\}$$

$$T_S = [N(x)]\{T_S\} \tag{3.3}$$

where $[N(x)]$ are the element interpolation functions. Following usual finite element procedures (ref. 5), the discritized equations for an element of length L may be derived in the form

$$\begin{bmatrix} C_F & 0 \\ 0 & C_S \end{bmatrix} \begin{Bmatrix} \dot{T}_F \\ \dot{T}_S \end{Bmatrix} + \begin{bmatrix} K_v + K_A + K_F & -K_A \\ -K_A & K_S + K_R \end{bmatrix} \begin{Bmatrix} T_F \\ T_S \end{Bmatrix} = \begin{Bmatrix} 0 \\ Q \end{Bmatrix} \tag{3.4}$$

where the element capacitance matrices are given by

$$[C_F] = \int_0^L \rho_F c_F A_F \{N\}[N] dx$$

$$[C_S] = \int_0^L \rho_S c_S A_S \{N\}[N] dx \tag{3.5}$$

and the element conductance matrices are

$$[K_v] = \int_0^L \dot{m} c_F \{N\}[\frac{dN}{dx}] dx$$

$$[K_A] = \int_0^L wh \{N\}[N] dx$$

$$[K_F] = \int_0^L k_F A_F \left\{\frac{dN}{dx}\right\} \left[\frac{dN}{dx}\right] dx \tag{3.6}$$

$$[K_S] = \int_0^L k_S A_S \left\{\frac{dN}{dx}\right\} \left[\frac{dN}{dx}\right] dx$$

$$[K_R]\{T_S\} = \int_0^L \sigma \epsilon T^4 \{N\} dx$$

8

The element equations given in Eqs. (3.4) show that the coolant passage model can be regarded as an assembly of elements where each element represents a single heat transfer mode. Thus we can represent the coolant passage in terms of two convective elements: (1) a mass-transport element (Fig. 7a), and (2) a surface convection element (Fig. 7b). The mass transport element represents the downstream convective heat transfer due to mass flow; it has a capacitance matrix $[C_F]$ as well as conductance matrices $[K_v]$ and $[K_F]$. The surface convection element represents the convection heat exchange between the coolant fluid and the solid; it does not have a capacitance matrix, but it has a conductance matrix $[K_h]$ linking the solid and fluid nodes. These coolant passage elements are assembled into the finite element thermal model for the complete convectively cooled structure that has conduction elements, radiation elements, and surface elements for convection to a specified convective exchange temperature.

The unsteady thermal analysis is nonlinear because of temperature dependent thermal properties and surface radiation. The equations are solved by time marching with the Crank-Nicolson algorithm; at each time step, the nonlinear algebraic equations are solved by Newton-Raphson iteration.

4 Thermo–Viscoplastic Structural Analysis

Unified viscoplastic constitutive models have evolved, over the last twenty years, to provide means for analytically representing material response from the elastic through the plastic range including strain–rate dependent plastic flow, creep and stress relaxation. The theories are guided by physical considerations including dislocation dynamics and are based on the principles of continuum mechanics. The first multi–dimensional formulation of elastic–viscoplastic constitutive equations was due to Bodner and Partom. Since then a number of constitutive models have appeared; many of these theories are summarized in review articles that appear in reference 6. A NASA-Lewis sponsored research program (HOST) conducted by the Southwest Research Institute recently concluded a four year research effort (ref. 7-8) to further develop unified constitutive models for isotropic materials and to demonstrate their usefulness for analysis of high temperature gas turbine engines. One result of this study is material property data for nickel–based alloys over a wide temperature range. The unified models employed were those of Bodner-Partom and Walker.

Unified viscoplastic theories have been implemented by a number of finite element researchers. Under the NASA HOST program, the Walker model was implemented in the MARC finite element program (ref. 9) and used to analyze the thermo–viscoplastic response of a turbine blade under simulated flight conditions. In another recent finite element application (ref. 10), the Bodner-Partom and Walker theories were compared for a thin circular plate subject to highly localized, transient heating.

In this research the Bodner–Partom constitutive model is employed, and the finite element approach developed in reference 11 for the isothermal case is extended to include thermal effects. The behavior of a thermo–viscoplastic structure subjected to aerodynamic heating is analyzed assuming that: (1) thermo–mechanical coupling in the conservation of energy equation can be neglected, (2) the structural response is quasi–static, and (3) deformations are infinitesimal. With these assumptions, an unsteady thermal analysis may be performed first to determine the temperatures. Then, using these temperatures, the structure's viscoplastic response is determined. The solution is thus obtained by separately solving initial boundary value problems for first the thermal and then the structural response.

4.1 Initial Value Viscoplasticity Problem

Consider a viscoplastic structure occupying a region Ω with boundary $\partial\Omega$. The behavior of the structure is described by the following system of differential equations:

1. Equilibrium in rate form,

$$\dot{\sigma}_{ij,j} + \dot{b}_i = 0 \tag{4.1}$$

where σ_{ij} is the stress tensor, b_i are the body forces per unit volume, and the summation convention is employed.

2. Kinematic relation for velocity gradients,

$$\dot{\epsilon}_{ij} = \dot{\epsilon}_{ij}^E + \dot{\epsilon}_{ij}^P = \frac{1}{2}(\dot{u}_{i,j} + \dot{u}_{j,i}) \tag{4.2}$$

where ϵ_{ij} is the total strain and superscripts E and P denote elastic and inelastic strain components, respectively. The displacement rates are $\dot{u}_i$.

3. Constitutive relations

$$\dot{\sigma}_{ij} = E_{ijkl}\dot{\epsilon}_{kl}^E - E_{ijkl}\alpha_{kl}\Delta\dot{T}$$

$$\dot{\epsilon}_{ij}^P = f_{ij}(\sigma_{ij}, Z_k) \qquad \text{(no sum)} \tag{4.3}$$

$$\dot{Z}_i = g_i(\sigma_{ij}, Z_k) \qquad \text{(no sum)}$$

where E_{ijkl} is Hooke's tensor of elasticity parameters, and α_{kl} is a tensor of thermal expansion parameters, and $\Delta\dot{T}$ represents the rate of the change in temperature from a reference temperature. Both E_{ijkl} and α_{kl} are temperature dependent. The constitutive functions are f_{ij} and g_i where Z_k represents internal state variables. These functions and state variables characterize the viscoplastic response of the material.

The description of the problem is completed by prescribing the boundary and initial conditions,

$$\dot{u} = \dot{\bar{u}}_i \quad on \quad \partial\Omega_1$$

$$\tag{4.4}$$

$$\dot{\sigma}_{ij}n_j = \dot{\bar{\sigma}}_i \quad on \quad \partial\Omega_3$$

11

where $\dot{\bar{u}}_i$ are prescribed surface displacement rates, n_j are the components of a unit normal vector, and $\dot{\bar{\sigma}}_i$ are prescribed surface traction rates. The initial conditions include specifying the displacements, stresses and internal state variables, i.e.

$$u_i(\mathbf{x}, 0), \sigma_{ij}(\mathbf{x}, 0), Z_i(\mathbf{x}, 0).$$

4.2 Constitutive Model

We now describe the explicit forms (ref. 6-7) of the Bodner-Partom constitutive equations used in the thermo–viscoplastic analysis. The Bodner-Partom constitutive model is of the internal state variable type that is a phenomenological theory based on the physical concepts related to dislocation dynamics. The model has gone through several modifications and extended for anisotropic work hardening materials. The current model also includes temperaure effects.

1. Flow Law,

   For the inelastic strain rate component, the isotropic form of the Prandtl-Reuss law is assumed

   $$\dot{\epsilon}_{ij}^P = \lambda S_{ij}$$

   $$\dot{\epsilon}_{kk}^P = 0 \qquad \lambda > 0$$

   (4.5)

   where S_{ij} are the deviatoric stress components given by

   $$S_{ij} = \sigma_{ij} - \frac{1}{3}\delta_{ij}\sigma_{kk}$$

   (4.6)

   $\dot{\epsilon}_{kk}^P = 0$ denotes plastic incompressibility.

2. Kinematic Equations,

   Squaring Eq.(4.5) leads to

   $$\lambda^2 = D_2^P / J_2$$

   (4.7)

   where D_2^P and J_2 are the strain rate and deviatoric stress invariants. The deviatoric stress invariant is

   $$J_2 = \frac{1}{2}S_{ij}S_{ij}$$

   (4.8)

The relation governing inelastic deformations is the "kinetic equation", and the form taken by Bodner-Partom is

$$D_2^P = D_0^2 \, exp[-(Z^2/3J_2)^n]$$ (4.9)

where D_o is the limiting strain rate in shear, n is a material constant, and Z is interpreted as a load history dependent parameter (herein called the internal state variable) that represents the hardened state of the material with respect to resistance to plastic flow. Combining Eqs.(4.5), (4.7), and (4.8) gives

$$\dot{\epsilon}_{ij}^P = \frac{S_{ij}}{\sqrt{J_2}} D_o exp\left[-\frac{1}{2}(Z^2/3J_2)^n\right]$$ (4.10)

3. Evolution Equations of Internal State Variable,

The internal state variable Z consists of isotropic and directional components,

$$Z = Z^I + Z^D$$ (4.11)

The evolution equation proposed for the isotropic hardening component (ref. 6) is

$$\dot{Z}^I(t) = m_1[Z_1 - Z_I(t)]\dot{W}_p(t) - A_1 Z_1 \left[\frac{Z^I(t) - Z_2}{Z_1}\right]^{r_1}$$ (4.12)

13

with the initial condition, $Z^I(0) = Z_0$. In the first term, Z_1 is the limiting (saturation) value of Z^I, m_1 is the hardening rate, and the plastic work rate is

$$\dot{W}p = \sigma_{ij}\dot{\epsilon}_{ij}^P \qquad (4.13)$$

which is taken as the measure of hardening. Z_2 is the minimum value of Z^I at a given temperature, and A_1 and r_1 are temperature dependent material constants.

The evolution form of the directional hardening component (ref.6) is defined as

$$Z^D(t) = \beta_{ij}(t)u_{ij}(t) \qquad (4.14)$$

where u_{ij} are the direction cosines of the current stress state,

$$u_{ij} = \sigma_{ij}(t)/[\sigma_{kl}(t)\sigma_{kl}(t)]^{\frac{1}{2}} \qquad (4.15)$$

The evolution equation for $\beta_{ij}(t)$ has the same general form as that for isotropic hardening but has tensorial character,

$$\dot{\beta}_{ij}(t) = m_2[Z_3 u_{ij}(t) - \beta_{ij}(t)]\dot{W}_p(t)$$
$$- A_2 Z_1 \left\{ \frac{[\beta_{kl}(t)\beta_{kl}(t)]^{\frac{1}{2}}}{Z_1} \right\}^{r_2} v_{ij}(t) \qquad (4.16)$$

where

$$v_{ij}(t) = \beta_{ij}(t)/[\beta_{kl}(t)\beta_{kl}(t)]^{\frac{1}{2}} \qquad (4.17)$$

and

$$\beta_{ij}(0) = 0 \qquad (4.18)$$

As in Eq.(4.12), m_2 is the hardening rate. A_2 and r_2 are temperature dependent material constants.

14

Other variants of the isotropic and directional hardening variables are described in refs.(6-8).

4.3 Finite Element Formulation

In this section, the finite element formulation for the initial value thermo–viscoplasticity problem (Section 4.1) is described. The development follows the approach of Ref. 11, and the details of the weak formulation are presented there. Since the discussion presented in Ref. 11 is for the isothermal case, this formulation extends the previous approach by the inclusion of temperature effects.

The finite element approach approximates displacement rates within an element by taking the displacement rates as

$$\{\dot{u}\} = [N]\{\dot{\delta}\} \tag{4.19}$$

where $[N]$ are the interpolation functions, and $\{\dot{\delta}\}$ represent the nodal displacement rates. Using the strain-displacement equations in rate form, Eq. 4.2, an element's strain rates can be computed from Eq. 4.19 as

$$\{\dot{\epsilon}\} = [B]\{\dot{\delta}\} \tag{4.20}$$

where $[B]$ is the strain–displacement matrix. Following usual finite element procedures, we can form the finite element equations for a typical element as,

$$[K(T)]\{\dot{\delta}\} = \{\dot{F}_p\} + \{\dot{F}_T\} + \{\dot{F}_\sigma\} + \{\dot{F}_B\} \tag{4.21}$$

where $[K(T)]$ is the element stiffness matrix, and the terms on the right–hand side are element load vectors due to the rate of plastic strains, temperature, surface tractions and body forces, respectively. These matrices are defined by

$$[K(T)] = \int_{\Omega_e} [B]^T [E(T)][B] d\Omega \tag{4.22}$$

$$\{\dot{F}_p\} = \int_{\Omega_e} [B]^T [E(T)]\{\dot{\epsilon}^p\} d\Omega \tag{4.23}$$

15

$$\{\dot{F}_T\} \; = \; \int_{\Omega_e} [B]^T [E(T)]\{\alpha(T)\}\Delta\dot{T}d\Omega \qquad (4.24)$$

$$\{\dot{F}_\sigma\} \; = \; \int_{\partial\Omega_e} [N]^T\{\ddot{\sigma}\}ds \qquad (4.25)$$

$$\{\dot{F}_B\} \; = \; \int_{\Omega_e} [N]^T\{\dot{b}\}d\Omega \qquad (4.26)$$

where Ω_e denotes the element volume, and $\partial\Omega_e$ denotes an element surface where tractions are defined.

The temperature affects the viscoplastic structural analysis directly in three ways: (1) the elasticity matrix $[E(T)]$ and the coefficients of thermal expansion $\{\alpha(T)\}$ depend on temperature, (2) nodal loads $\{\dot{F}_T\}$ depend on the local temperature rates, and (3) several parameters (see section 4.2) in the Bodner Partom constitutive model are temperature dependent.

4.4 Viscoplastic Solution Method

Since the present approach uses an uncoupled (sometimes called one-way coupled) formulation. the thermal problem is solved first followed by the viscoplastic analysis. The transient thermal problem is solved by time marching with a time step Δt_T, and the nodal temperatures at successive times $t_1, t_2, \cdots$ are obtained. These temperature vectors are used as input to the structural analysis.

The first computation in the structural analysis is to solve an initial statics problem if the initial temperature distribution $T(\mathbf{x}, 0)$ is not equal to a uniform reference temperature. The results of this analysis are the initial conditions (displacements and stresses) for the transient viscoplastic analysis. .

The viscoplastic analysis time–marches with a time step Δt_s. Experience has shown the time step required for the structural analysis is smaller than for the thermal analysis, i.e. $\Delta t_s < \Delta t_T$. At intermediate times in the structural analysis, the temperatures are linearly interpolated from the temperatures known at the beginning and end of the larger thermal time intervals.

The strategy employed in the viscoplastic algorithm is as follows: with the initial distribution of stress, temperature and internal variables specified use the equilibrium condition (Eq. 4.21) to obtain the nodal displacement rates. Then integrate the constitutive equations forward in time at the element Gauss integration points. With updated values of

16

the stress, temperature and internal variables at the new time, the equilibrium equation is solved again. This sequence of determining the nodal displacement rates, then advancing the constitutive equations in time is continued until the desired history of the initial boundary–value problem has been obtained.

Thus, the algorithm proceeds through the following steps:

1. At time t, initialize σ_{ij}, Z_i for each element;

2. Calculate $\dot{\epsilon}_{ij}^P = f_{ij}(\sigma_{ij}, Z_k)$ for each element;

3. Assemble and solve $[K]\{\dot{\delta}\} = \{\dot{F}\}$;

4. Calculate $\dot{\epsilon}_{ij}$ for each element, $\{ \dot{\epsilon}\} = [B]\{\dot{\delta}\}$;

5. Calculate $\dot{\sigma}_{ij}$ for each element, $\{\dot{\sigma}\} = [E]\{\dot{\epsilon} - \dot{\epsilon}^P\} - [E]\alpha\Delta\dot{T}$;

6. Calculate $\dot{Z}_i$ for each element, $\dot{Z}_i = g_i(\sigma_{ij}, Z_k)$;

7. Integrate $\dot{\sigma}_{ij}, \dot{Z}$ forward for each element to get σ_{ij} and Z_i at $t + \Delta t_s$;

8. If $t + \Delta t_s < t_{final}$ go to 2, otherwise stop.

The computational method above has been presented for a constant time step Δt_s. Computational experience by several investigators (see Ref. 8, 10–11) indicates that a very small time step can be required because of the "stiff" nature of the ordinary differential equations describing the internal state variables. To gain improved efficiency and reliability a variable time step algorithm has been implemented and will be described.

4.5 Variable Time Step Algorithm

In the constant time step viscoplastic algorithm the internal state variables are advanced in time with the conditionally stable Euler forward difference algorithm. The variable time step algorithm is a modified Euler scheme using a truncation error criterion (Ref. 12) to adjust the time step.

For simplicity, consider the single ordinary differential equation,

$$\dot{y} = f(y, t) \tag{4.27}$$

17

The solution is advanced using a predictor–corrector scheme. The predictor phase consists of an Euler step:

$$y^P_{t+\Delta t} = y_t + \Delta t \dot{y}_t \tag{4.28}$$

$$\dot{y}^P_{t+\Delta t} = f(y^P_{t+\Delta t}, t + \Delta t) \tag{4.29}$$

An error indicator E (Ref. 12) is then computed from

$$E = \frac{|\Delta t(\dot{y}^P_{t+\Delta t} - \dot{y}_t)|}{2|y^P_{t+\Delta t}|} \tag{4.30}$$

The error indicator is next compared with a preset error criterion, and if the criterion is met, the time step is sufficiently small enough to proceed to the corrector stage. Otherwise, the predictor phase Eqs. (4.28–4.29) is repeated with a smaller time step.

The corrector phase is the modified Newton scheme,

$$\dot{y}_{avg} = (\dot{y}_t + \dot{y}^P_{t+\Delta t})/2 \tag{4.31}$$

$$y^C_{t+\Delta t} = y_t + \Delta t \dot{y}_{avg} \tag{4.32}$$

A flow chart depicting the adaptive scheme is shown in Fig. 8. The flow chart shows how the time step is either reduced or increased depending on the error indicator, Eq. (4.30).

18

5 Viscous Flow Analysis

Finite element analysis of compressible flows is a relatively new development, but significant progress has been made in the last few years. Computational techniques were developed first for inviscid flows, and then the techniques were extended for viscous flows. The first successful algorithms were explicit schemes; current research is focused on the development of implicit schemes. In this report we describe an explicit finite element algorithm (ref. 13) that is used to solve the Navier-Stokes equations for the external flow. A basic objective of the flow analysis is to predict the aerothermal loads acting on the structure, i.e. the surface heating rate, the skin function (shearing stress), and pressure needed for the thermal-structural analysis.

5.1 Problem Formulation

A laminar compressible flow with a calorically perfect gas is assumed. The Navier-Stokes equations are written in the conservation form,

$$\frac{\partial \{U\}}{\partial t} + \frac{\partial \{E_I - E_V\}}{\partial x} + \frac{\partial \{F_I - F_V\}}{\partial y} = 0 \tag{5.1}$$

where $\{U\}$ is the vector of conservation variables; $\{E_I\}$ and $\{F_I\}$ are inviscid flux components; $\{E_V\}$ and $\{F_V\}$ are viscous flux components. These vectors are given by

$$\{U\}^T = [\rho \quad \rho u \quad \rho v \quad \rho E_t]$$

$$\{E_I\}^T = [\rho u \quad \rho u^2 + P \quad \rho uv \quad (\rho E_t + P)u]$$

$$\{F_I\}^T = [\rho v \quad \rho vu \quad \rho v^2 + P \quad (\rho E_t + P)v] \tag{5.2}$$

$$\{E_V\}^T = [0 \quad \sigma_{xx} \quad \tau_{xy} \quad u\sigma_{xx} + v\tau_{xy} - q_x]$$

$$\{F_V\}^T = [0 \quad \tau_{xy} \quad \sigma_{yy} \quad u\tau_{xy} + v\sigma_{yy} - q_y]$$

where ρ is the fluid density, u and v are velocity components, E_t is the total energy; σ_{xx}, σ_{yy} and τ_{xy} are stress components; and q_x, q_y are heat fluxes. In the inviscid flux components

19

the pressure P is defined for a perfect gas as

$$P = (\gamma - 1)\rho[E_t - (u^2 + v^2)/2] \tag{5.3}$$

where γ is the ratio of specific heats. In the viscous terms, the stress components are related to the velocity gradients by

$$
\begin{aligned}
\sigma_{xx} &= \tfrac{2}{3}\mu(T)(2\tfrac{\partial u}{\partial x} - \tfrac{\partial v}{\partial y}) \\
\tau_{xy} &= \mu(T)(\tfrac{\partial u}{\partial y} + \tfrac{\partial v}{\partial x}) \\
\tau_{yy} &= \tfrac{2}{3}\mu(T)(2\tfrac{\partial v}{\partial y} - \tfrac{\partial u}{\partial x})
\end{aligned}
\tag{5.4}
$$

where T is temperature. The heat fluxes are computed by Fourier's law

$$
\begin{aligned}
q_x &= k(T)\tfrac{\partial T}{\partial x} \\
q_v &= -k(T)\tfrac{\partial T}{\partial y}
\end{aligned}
\tag{5.5}
$$

The temperature dependent viscosity is computed from Sutherland's law, and the thermal conductivity is computed assuming a Prandtl number, $Pr = 0.72$.

Equation (5.1) is solved subject to appropriate initial and boundary conditions. Consider a domain Ω bounded by a surface $\partial\Omega$. The initial conditions consist of specifying the distributions of the conservation variables at time zero. Typical boundary conditions may include: (1) specifying all conservation variables for supersonic inflow on a segment of the boundary $\partial\Omega_1$, (2) requiring that $\vec{V} \cdot \hat{n} = 0$ on a symmetry plane, $\partial\Omega_2$ ($\vec{V}$ is the velocity vector, and $\hat{n}$ is a unit normal vector) and specifying the heat flux normal to the surface $\partial\Omega_2$ be zero, (3) using appropriate boundary conditions on a outflow surface $\partial\Omega_3$, and (4) specifying $\vec{V} = 0$ and the surface temperature T on aerodynamic surfaces, $\partial\Omega_4$. On supersonic outflow surfaces, the finite element formulation supplies appropriate natural boundary conditions consisting of surface integrals of flux components.

5.2 Taylor-Galerkin Algorithm

For simplicity the solution algorithm will be given for the single scalar equation,

$$\frac{\partial u}{\partial t} + \frac{\partial}{\partial x}(E_I - E_V) + \frac{\partial}{\partial y}(F_I - F_V) = 0 \tag{5.6}$$

where the variables, $u, E_I, F_I, E_V,$ and F_V are analogous to the corresponding vector quantities in Eq. (1). Let $\{u\}^n$ denote the element nodal values of the flow variable $u(x, y, t)$ at time t_n. The time step Δt spans two typical times t_n and t_{n+1} in the transient response. The computation proceeds through two time levels $t_{n+\frac{1}{2}}$ and t_{n+1}. At time level $t_{n+\frac{1}{2}}$, values for u that are constant within each element are computed explicitly. At time level t_{n+1}, the constant element values are used to compute nodal values for u.

Time Level $t_{n+\frac{1}{2}}$

A constant element value $u_{\Omega_e}^{n+\frac{1}{2}}$ is computed from

$$Au_{\Omega_e}^{n+\frac{1}{2}} = \int_{\Omega_e} [N]dA\{u\}^n - \frac{\Delta t}{2}\left[\int_{\Omega_e}\left[\frac{\partial N}{\partial x}\right]dA\{E_I - E_V\}^n\right.$$

$$\left. + \int_{\Omega_e}\left[\frac{\partial N}{\partial y}\right]dA\{F_I - F_V\}^n\right] \tag{5.7}$$

where A denotes the area of element Ω_e, and $[N]$ are the element interpolation functions. Quantities such as $\{E_I\}^n$ represent nodal values at time t_n.

Time Level t_{n+1}

Nodal values are computed from

$$[M]\{u\}^{n+1} = [M]\{u\}^n + \{R_1\}^{n+\frac{1}{2}} + \{R_2\}^{n+\frac{1}{2}} + \{R_3\}^n + \{R_4\}^n \tag{5.8}$$

where

$$[M] = \int_{\Omega_e} \{N\}[N]dA \tag{5.9}$$

21

and

$$\{R_1\}^{n+\frac{1}{2}} = \Delta t \left[\int_{\Omega_e} \left\{ \frac{\partial N}{\partial x} \right\} dA E_I^{n+\frac{1}{2}} + \int_{\Omega_e} \left\{ \frac{\partial N}{\partial y} \right\} dA F_I^{n+\frac{1}{2}} \right] \tag{5.10}$$

$$\{R_2\}^{n+\frac{1}{2}} = -\Delta t \int_{\partial\Omega_e} \{N\} ds \left[l(E_I)_s^{n+\frac{1}{2}} + m(F_I)_s^{n+\frac{1}{2}} \right] \tag{5.11}$$

$$\{R_3\}^n = -\Delta t \left[\int_{\Omega_e} \left\{ \frac{\partial N}{\partial x} \right\} [N] dA \{E_V\}^n + \int_{\Omega_e} \left\{ \frac{\partial N}{\partial y} \right\} [N] dA \{F_V\}^n \right] \tag{5.12}$$

$$\{R_4\}^n = \Delta t \int_{\partial\Omega_e} \{N\}[N] dS \left[l\{E_V\}_s^n + m\{F_V\}_s^n \right] \tag{5.13}$$

In Eqs. (5.11) and (5.13), l and m are the components of a unit vector normal to the boundary. The load vectors $\{R_2\}$ and $\{R_4\}$ represent natural conditions and are evaluated on ourflow surfaces.

The mass matrix $[M]$, Eq. (5.9), is diagonalized to yield a "lumped mass matrix" producing an explicit scheme where the new nodal values can be computed directly from Eq. (5.8).

5.3   Aerothermal Loads

Accurate computation of surface quantities such as heat fluxes is an important objective of the viscous flow analysis. By Fourier's law, heat fluxes may be computed from temperature derivatives at the fluid/solid interface. In typical elements, temperatures vary linearly, and temperature gradients normal to the interface are constant. Heat fluxes computed from these derivatives are not sufficiently accurate, and conservation is not guaranteed. As an alternate approach, a finite element scheme based on Eq.(5.8) is used. This latter approach does not require the computation of temperature derivatives, and conservation is guaranteed.

We will illustrate the approach for surface heat fluxes, but skin friction can be computed in a similar fashion. For heat fluxes, we use the conservation of energy equation assuming the computation has reached steady state, i.e. $\{u\}^{n+1} = \{u\}^n$. On no-slip boundary surfaces where normal heat fluxes are to be computed, Eq. (5.8) reduces to

$$\{R_3\} + \{R_4\} = 0$$

since the inviscid fluxes in the energy equation are zero on the no–slip boundary. Substituting for $\{R_3\}$ using Eq. (5.10) and evaluating $\{R_4\}$ at the surface produces

$$
\begin{aligned}
\int_{\partial\Omega}\{N\}[N]ds\{q_n\} \;=\;& \int_{\Omega_e}\left\{\frac{\partial N}{\partial x}\right\}[N]dA\{E_V\} \\
&+ \int_{\Omega_e}\left\{\frac{\partial N}{\partial y}\right\}[N]dA\{F_V\}
\end{aligned}
\tag{5.14}
$$

where $\{q_n\}$ are nodal heat fluxes for an element. To aid in the computation, the coefficient matrix for $\{q_n\}$ in this equation can be diagonalized to produce an explicit scheme for directly computing the nodal heat fluxes.

6 Recent Numerical Results

Presented here are some recent numerical results illustrating progress in code development and progress in understanding basic F-T-S interaction phenomena for hypersonic structures.

6.1 Thermo–Viscoplastic Structural Computations

6.1.1 Simplified Model

To gain a preliminary understanding of the behavior of a convectively cooled structure subjected to convective heating, a simple 1D bar model was investigated. A segment (Fig. 9a) of the aerodynamic skin is modeled assuming uniform temperature. The coolant is assumed to have a constant, specified temperature, and the skin is heated convectively. A strong time variation of the convection coefficient, (Fig. 9b) simulates the passage of a moving shock. The resulting transient temperature and bar compressive stress exhibit features to be expected in a more complex model.

The transient temperature history (Fig. 10a) shows a rapid rise following the sudden increase in the convective coefficient, and then a smooth decay after the large convective heating is removed. The convective cooling causes the temperature to return quickly to equilibrium. The initial rapid increase in temperature causes the bar to yield in compression very early in the response (Fig. 10b). After the temperature begins to decay at $t = 0.5s$, the stress rapidly changes to tension hence as the temperature returns to equilibrium a large residual tensile stress remains in the bar. The tensile stress is induced because the initial high temperature causes the bar to expand which induces compressive yielding. This yielding tends to permanently shorten the bar. However, the bar's fixed end boundary conditions prohibit the bar from changing in length so that a tensile stress develops as the material cools.

In the initial viscoplastic analysis a fixed time step of 0.001 s was used, and 1200 time steps were required for the analysis. The variable time step algorithm was then implemented, and the problem was resolved. Fig. 10c shows the history of the variable time step and indicates that the new analysis required only 213 steps — a substantial savings. The figure shows that in the "flat" part of the stress response a large time step was used, but near $t = 0$ and again at $t = 0.5s$ when the stress is changing rapidly, small time steps are needed to capture the response accurately. This example shows that the adaptive time step algorithm is an important step towards producing an efficient, accurate

24

solution.

6.1.2 Convectively Cooled Structure

A more realistic 2D model of a convectively cooled hypersonic structure is shown in Fig. 11. The model represents a segment of a convectively cooled structure such as a wall of a scramjet engine fuel injection strut. The finite element thermal model (Fig. 11a) includes: (1) conduction heat transfer in the aerodynamic skin and primary structure, (2) convective heat transfer between the walls of the coolant passage and coolant, (3) mass transport convection in the coolant which has an unknown bulk temperature, and (4) surface radiation on the aerodynamic skin. The aerodynamic skin is uniformly convectively heated over its length, and superimposed on the uniform heating is a local, intense heating simulating a transient shock. The transient heating is induced by the time–dependent convection coefficient shown in Fig. 11b. Thermal properties and data are tabulated in Table 1. The properties are representative of a high temperature nickel superalloy.

In the plane strain finite element model, the primary structure and aerodynamic skin have unit thickness, but the heat exchanger in the coolant passage has a thickness of 0.1 in. to provide an effective structural stiffness. The wall segment has fixed displacement boundary conditions at the left and right ends. Data for the Bodner-Partom viscoplastic model are tabulated in Table 2.

The thermal response of the wall segment is shown in Fig. 12. Figure 12a shows the time history of a point on the aerodynamic skin directly under the transient heating; Fig. 12b shows contours of temperatures at $t = 0.5s$ when temperatures are maximum. The temperature history is qualitatively similar to the results obtained in the 1D model showing the rapid skin temperature rise and fall with the simulated shock heating. The temperature contours show relatively steep thermal gradients induced by the local heating, and that the coolant substantially limits the extent of the induced high temperatures. Thus the high temperatures are confined to the aerodynamic skin, and the primary structure experiences only small temperature changes. The temperature gradients in the skin particularly at the coolant–skin interface are not predicted with high accuracy because of the engineering model of the coolant heat transfer. However, local temperature levels in the skin are reasonably accurate since net energy transfer to the coolant is modeled satisfactorily.

Stress histories at three points through the skin thickness are shown in Fig. 13. The stress histories follow the temperature, and under the intense local heating stresses are very similar to the results obtained from the 1D model. At this location the skin yields

through most of its thickness. After the heating ceases there is a rapid decay of stress, and under the intense local heating there are residual tensile stresses.

The viscoplastic stress histories are compared with stresses predicted assuming elastic behavior in Fig. 14. The elasticity assumption is clearly not permissable because predicted stresses are too high, and, of course, no residual stresses are predicted. Deformations (not shown) predicted by the elastic model are also too small.

The two dimensional character of the stress components σ_x and σ_y are shown in Figs. 15 and 16, respectively. The stress distributions are shown at three times ($t = 0.1s, 0.5s, 1.0s$) in the response. The stresses at the $t = 1.0s$ are the residual stresses. The figures show that in addition to the high σ_x stresses induced in the skin that cause yielding, there are also high stresses in the heat exchanger region. Although the structural model of the heat exchanger region is crude, high tensile stresses σ_y can potentially cause a bond failure at the heat exchanger/skin joint. Such a failure would cause a loss of heat transfer between the skin and heat exchanger resulting in excessively high skin temperatures. This is a possible failure mode that needs further investigation.

The deformed structure and principal plastic strains at $t = 0.5s$ are shown in Fig. 17 and 18, respectively. Peak deformations are relatively small, but the effect of internal coolant pressure was neglected. The effect of this pressure on deformation and plastic strain needs to be evaluated.

6.2 Flow Computations

6.2.1 Flow Over Flat Plate

To validate the viscous flow code and to assess mathematical models for artificial dissipation the problem of supersonic flow over a flat plate was solved. This problem has been solved by several investigators starting with Carter (NASA TR R-385) who obtained a numerical solution using a finite difference scheme. The problem statement is shown in Fig. 19a. The mesh from adaptive refinement of the finite model is shown superimposed on density contours in Fig. 19b. Temperature profiles at the exit plane are shown in Fig. 19c. The temperature profiles shown are, in general, not representative of high speed flows because of the high wall temperature boundary condition. In reviewing the results from several different artificial dissipation models, the McCormack-Baldwin model gives slightly superior results to those obtained with Lapidus dissipation, but it is more expensive since it requires extraction of second derivatives of the pressure. The successful solution of

26

the Carter problem demonstrates that the basic algorithm is working effectively, but work remains to be done to validate the code for higher Mach number flows with stronger viscous effects.

6.2.2 Boundary Layer Flow

To further evaluate the viscous flow code, a high speed boundary layer flow over a flat plate is currently being analyzed. The problem statement is presented in Fig. 20a. The temperature profile at the inflow plant is shown in Fig. 20b. The profile shown is representative of high speed flows and must be predicted accurately for wall heating rates to be predicted well. An important role of this problem is to provide insight into the effect of artificial dissipation on the temperature distribution and the wall heating rates. Artificial dissipation tends to cause boundary layers to be too thick, distorts temperature profiles and can adversely affect wall heating rate predictions. The computed temperature profile at the outflow plane in Fig. 20b shows only small effects of artificial dissipation, but heating rates (not shown) computed from this solution are below the expected values. Work on this problem is in progress. The results so far indicate that as the level of artificial dissipation is reduced, the wall heating rates will improve in accuracy. Successful completion of this problem will mean that the integration of the flow analysis with a deformed structure can be initiated.

27

7 Research Forecast

In this initial contract year, the basic computational schemes for solving a strong F-T-S interaction problem have been developed assuming structural temperatures are below the melting point. In the next year, a major goal will be to integrate the components to solve a problem with a complete F-T-S interaction. Specific objectives for the next year are:

1. Further enhancement of the thermo–viscoplasticity code to provide:

   (a) adaptive mesh refinement

   (b) inclusion of state variables in the constitutive model to incorporate material damage

2. Further development of the viscous flow code to predict aerodynamic heating rates, surface pressures and shearing stresses.

3. Development of a mesh movement algorithm for interfacing flow meshes with the mesh for the deformed structure.

4. Numerical solutions for:

   (a) thermo–viscoplastic response of a convectively cooled structure with damage predictions for multiple loading cycles.

   (b) more difficult viscous flow problems with flow recirculations

5. Development of thermal–structural formulations for metallic materials where temperatures can exceed the melting temperature.

6. Presentation of a paper at the 30th AIAA Structures, Structural Dynamics, and Materials Conference to be held April 3-5, 1989 in Mobile, Alabama.

8 References

1. Wieting, A. R. and Holden, M. S.: "Experimental Study of Shock Wave Interference Heating on a Cylindrical Leading Edge," AIAA 22nd Thermophysics Conference, Honolulu, Hawaii, June 8–10, 1987, AIAA Paper 87-1511.

2. Dechaumphai, P., Thornton, E. A. and Weiting, A. R.: "Flow-Thermal-Structural Study of Aerodynamically Heated Leading Edges," AIAA/ASME/ASCE/AHS 29th Structures, Structural Dynamics and Materials Conference, Williamsburg, Virginia, April 18–20, 1988, AIAA Paper 88-2245.

3. Dechaumphai, P., Weiting, A. R. and Thornton, E. A.: "Thermal-Structural Performances of an Actively Cooled Leading Edge Subjected to Type IV Shock Wave Interference Heating," Third National Aero-Space Plane Symposium, June 2–4, 1987, Paper No. 24.

4. Melis, M. W. and Gladden, H. J.: "Thermostructural Analysis with Experimental Verification in a High Heat Flux Facility of a Simualted Cowl Lip," AIAA/ASME/ASCE/AHS 29th Structures, Structural Dynamics and Materials Conference, Williamsburg, Virginia, April 18–20, 1988, AIAA 88-2222.

5. Thornton, E. A. and Weiting, A. R.: "Finite Element Methodology for Transient Conduction/Forced Convection Thermal Analysis," *Progress in Astronautics and Acronautics: Heat Transfer, Thermal Control and Heat Pipes*, Vol. 70, Edited by Walter B. Olstad, AIAA, New York, pp. 77–103.

6. Miller, A. K. (editor), *Unified Constitutive Equations for Creep and Plasticity*, Elsevier Applied Science Publishers, 1987.

7. Chan, K. S., Lindholm, U. S., Bodner, S. R., Hill, J. R., Weber, R. M. and Meyer, T. G., "Constitutive Modeling for Isotropic Materials (HOST)," Third Annual Status Report, Southwest Research Institute, San Antonio, Texas, August, 1986, NASA CR 179522.

8. Chan, K. S., Lindholm, U. S. and Bodner, S. R., "Constitutive Modeling for Isotropic Materials (HOST), Final Report, Southwest Research Institute, San Antonio, Texas, June, 1988, NASA CR-182132.

9. MARC General Purpose Finite Element Program, MARC Corporation, Palo Alto, CA.

10. Chang, H. T. and Allen, D. H.: "Analysis of Viscoplastic Plates Subjected to Rapid External Heating," AIAA/ASME/ASCE/AHS 29th Structures, Structural Dynamics and Materials Conference, Williamsburg, Virginia, April 18–20, 1988, AIAA Paper 88-2422.

11. Bass, J. M. and Oden, J. T.: "Adaptive Finite Element Methods for a Class of Evolution Problems in Viscoplasticity," *Int.J.Eng.Sci.*, Vol. 25, No. 6, 1987, pp. 623–653.

12. Kumar, V., Morjaria, M. and Mukherjee, S., "Numerical Integration of Some Constitutive Models of Inelastic Deformation," J. Engineering Materials and Technology, Vol. 102, Jan. 1980, pp. 92–96.

13. Thornton, E. A., Dechaumphai, P. and Vemaganti, G., "A Finite Element Approach for Prediction of Aerothermal Loads," AIAA/ASME 4th Fluid Mechanics, Plasma Dynamics and Lasers Conference, Atlanta, GA, May 12–14, 1986, AIAA-86-1050.

EQUILIBRIUM SURFACE TEMPERATURES
$M_\infty = 8;\ q = 2200\ psf$
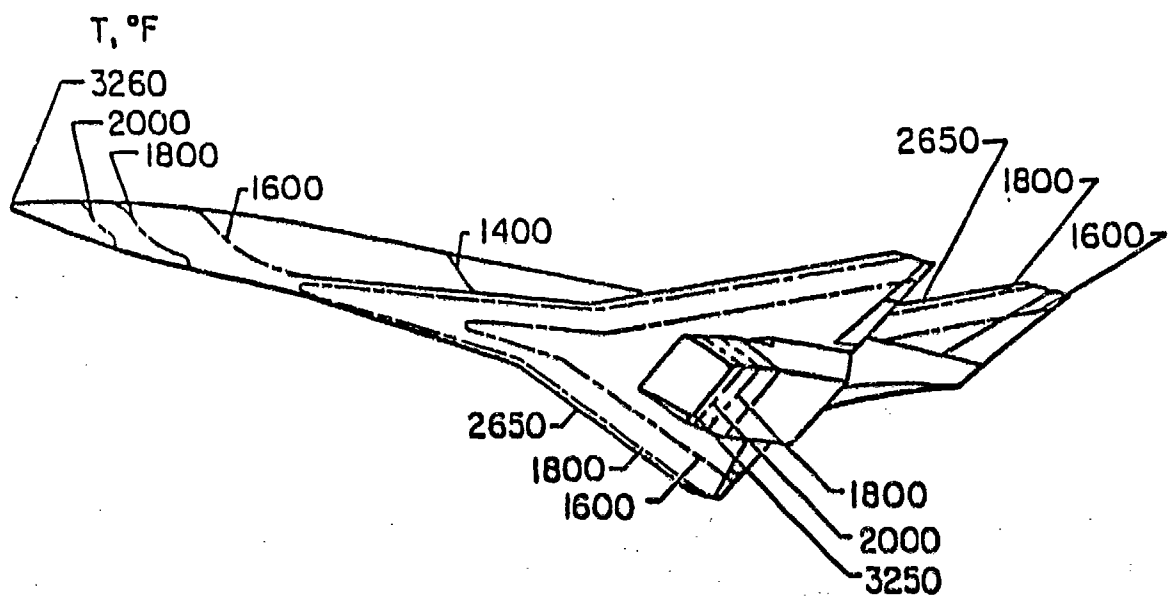
Figure 1: Estimated National Aerospace Plane Surface Temperatures (NASA TM 89143)
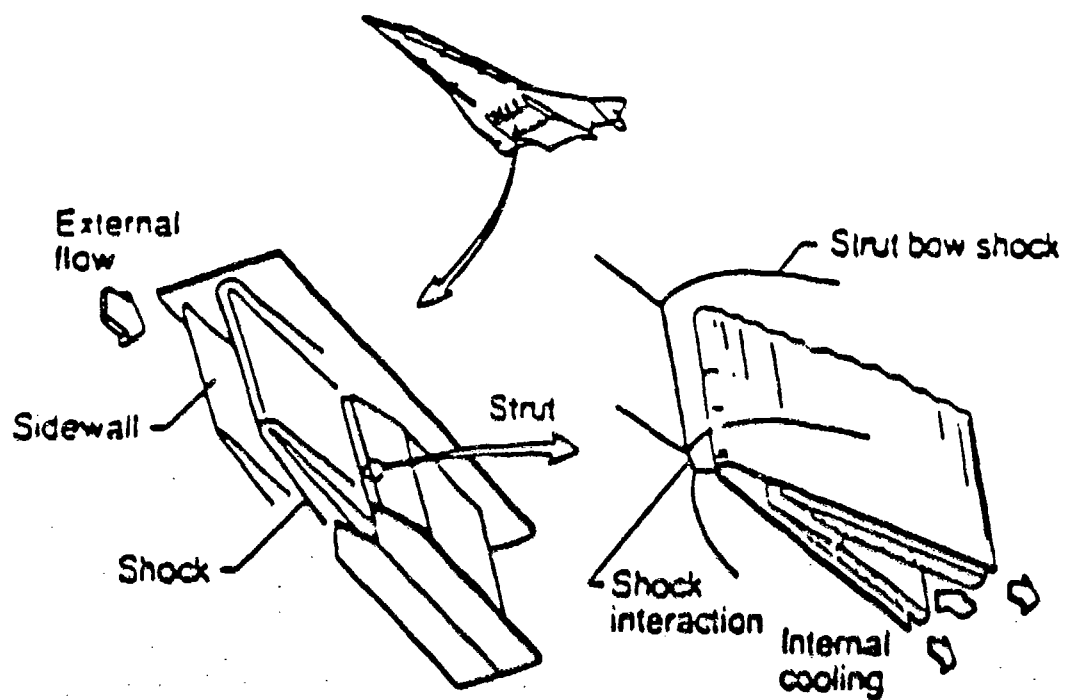
Figure 2: Fluid-thermal-structural Interactions on an Aerospace Plane Scramjet Engine Leading Edge
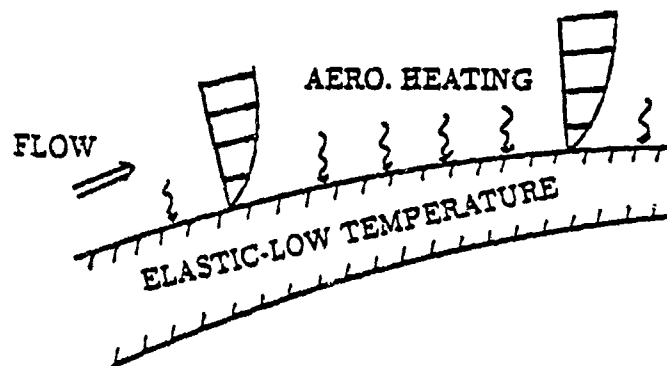
a) Aerodynamic Heating on Undeformed Structure
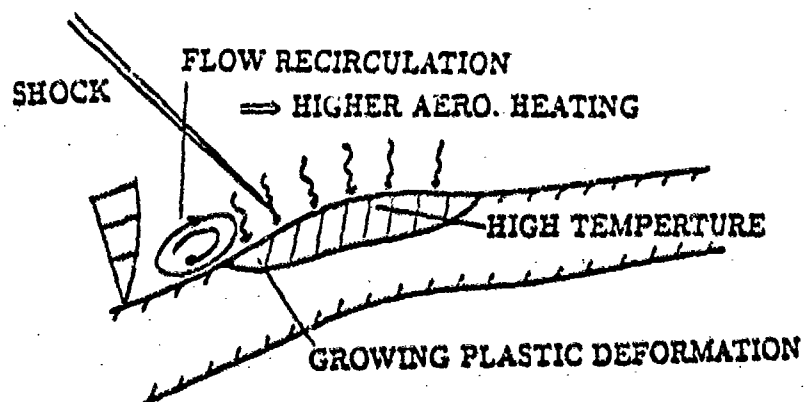
b) Plastic Deformation Induced by High Aerodynamic Heating on Deformed Structure

Figure 3: FTS Interactions in Hypersonic Flight
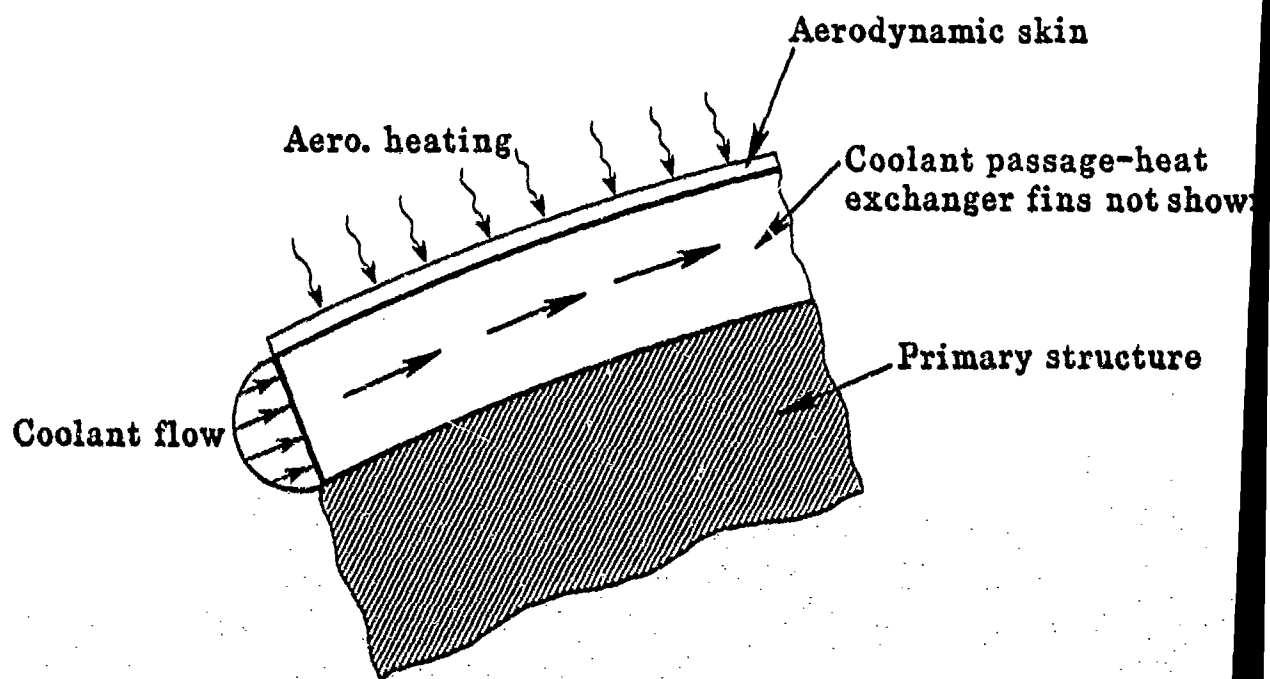
Figure 4: Convectively-cooled Structure
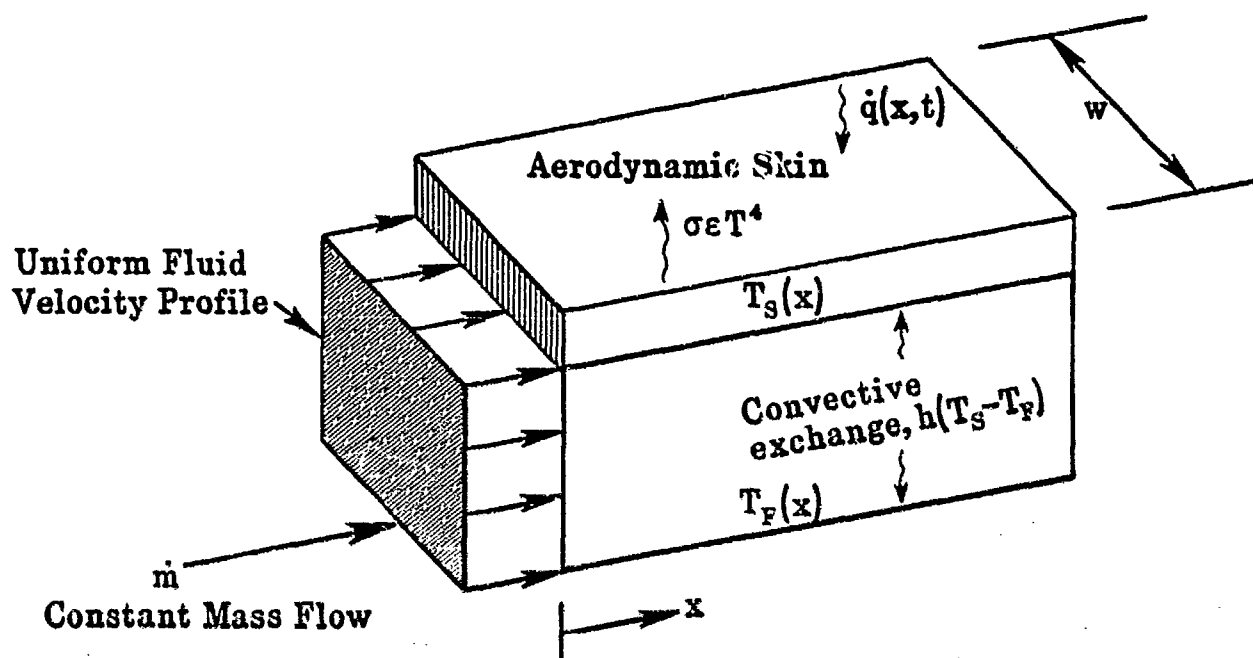
Figure 5: Engineering Model of Coolant Passage Heat Transfer
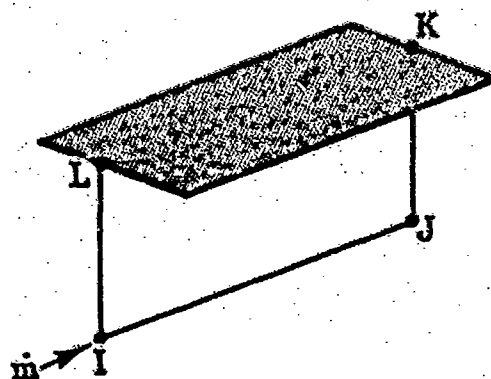
Figure 6: Finite Element Model of Coolant Passage
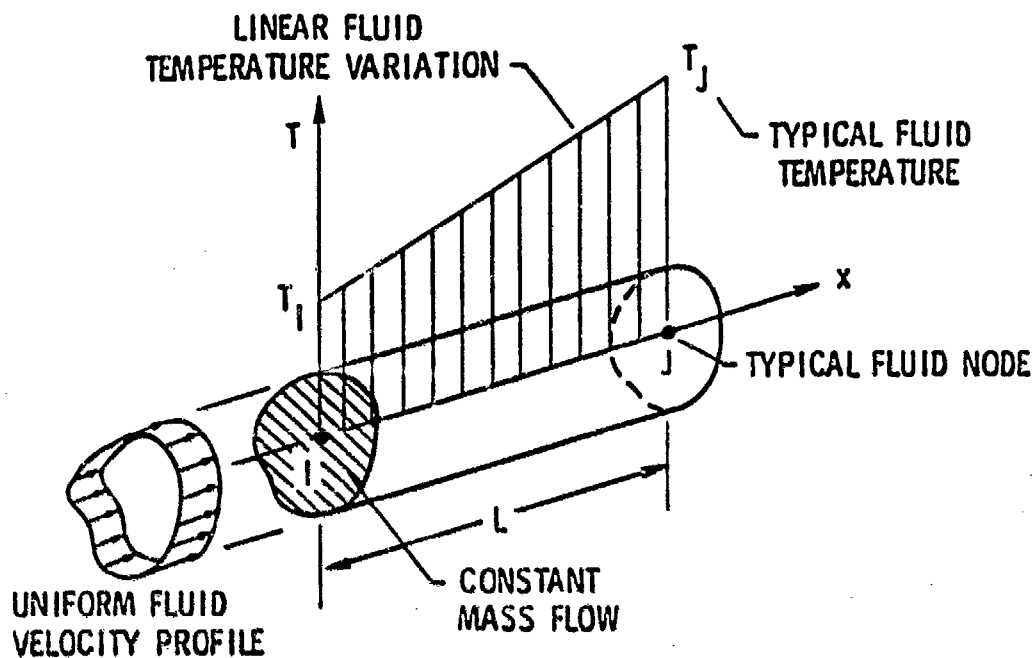
a) mass transport element
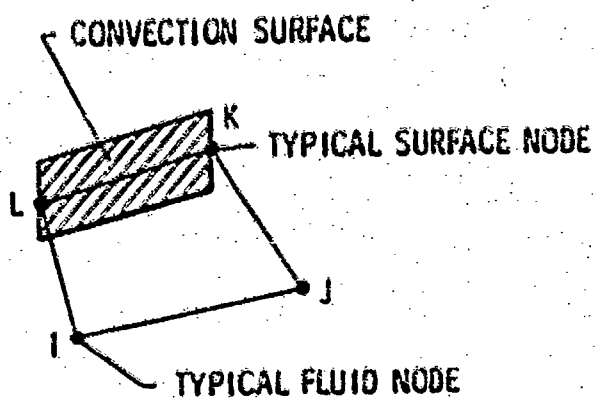
(b) surface convection element

Figure 7: Coolant Passage Convective Elements

START

PREDICTOR $\quad y_t^p + \Delta t, \ \dot{y}_t^p + \Delta t$

ERROR = E

E > MAX

YES

NO

$\Delta t = \Delta t / 2$

CORRECTOR $\quad \dot{y}_{avg}, \ y_{t+\Delta t}^c$

E < MIN

$\Delta t = 2 * \Delta t$

LAST Δt

NO

YES

STOP
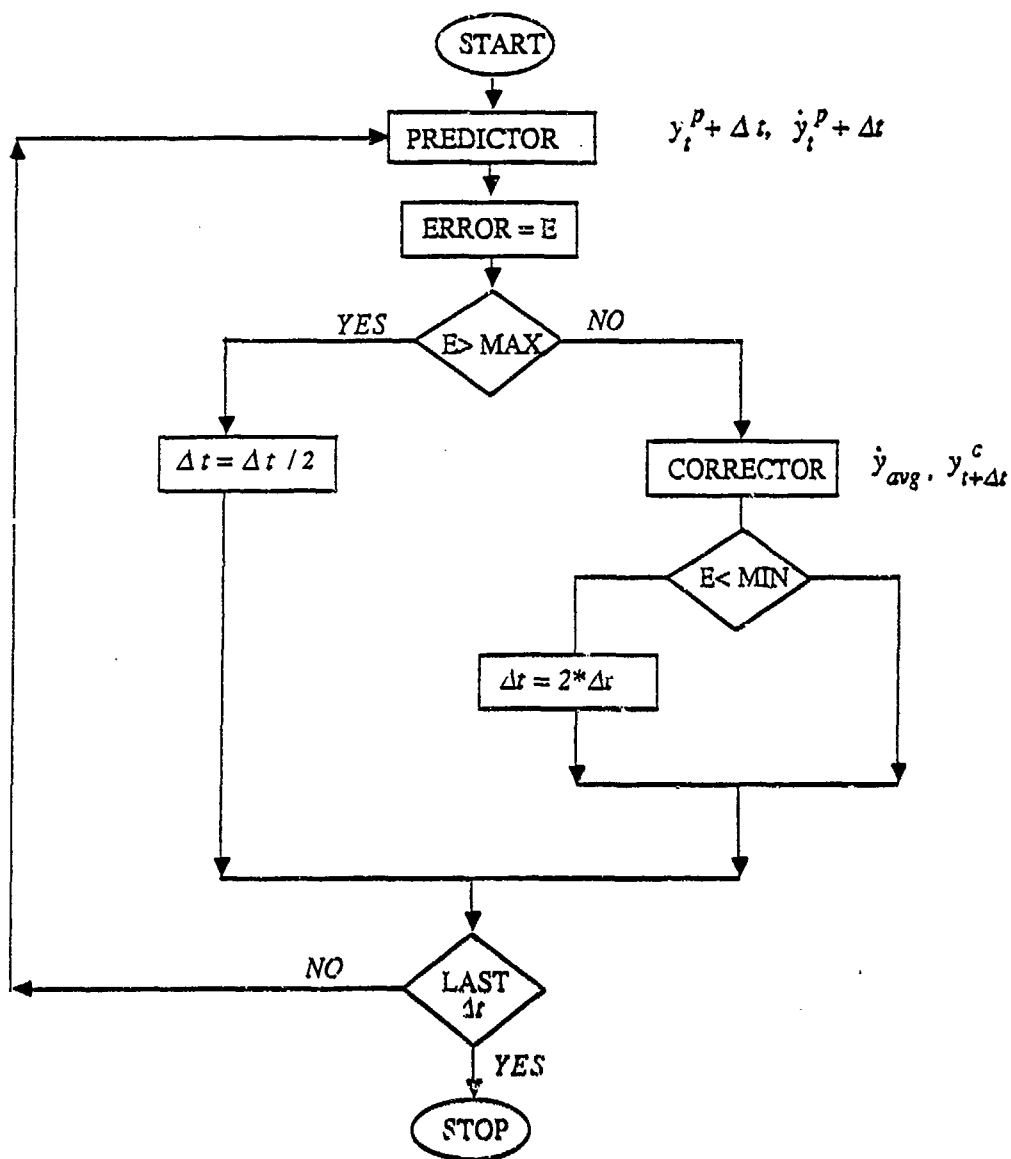
Figure 8: Flow Chart for Adaptive Time Step Algorithm
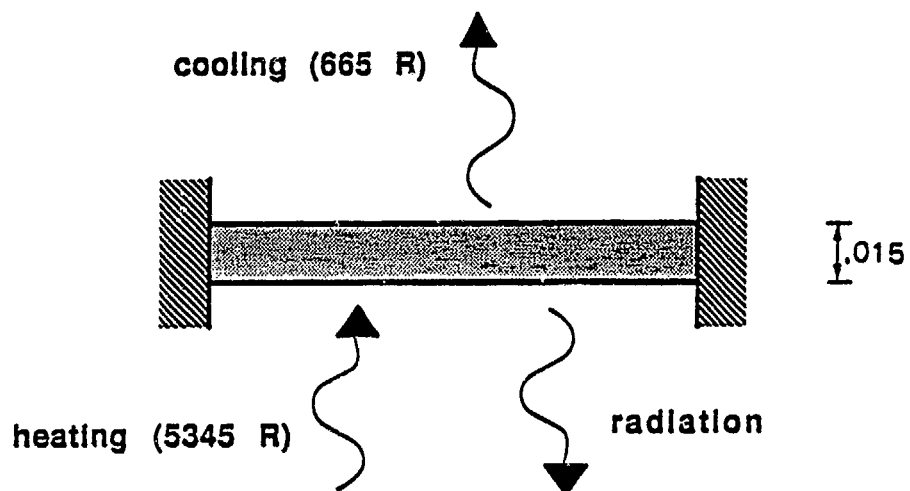
(a) Thermal-structural model
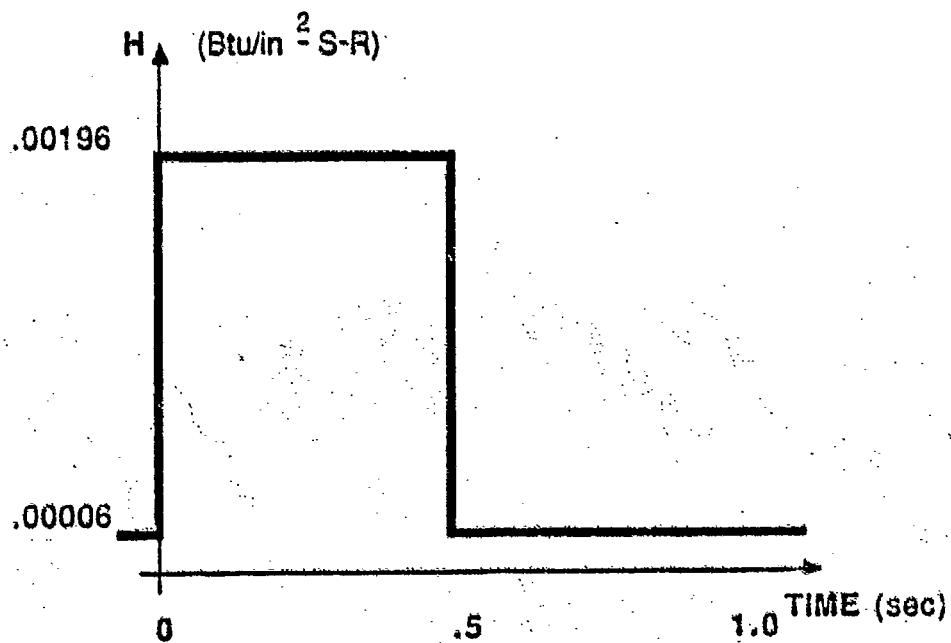
(b) Convection coefficient history

Figure 9: 1D Model of Convectively Cooled Structure

TEMPERATURE (R)

(a) Temperature history

STRESS (MPa)

(b) Stress history

DT (sec)

FIXED DT
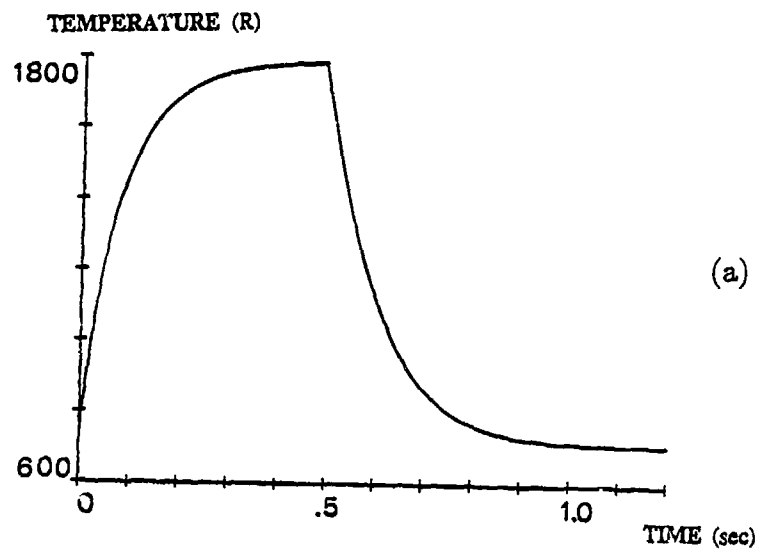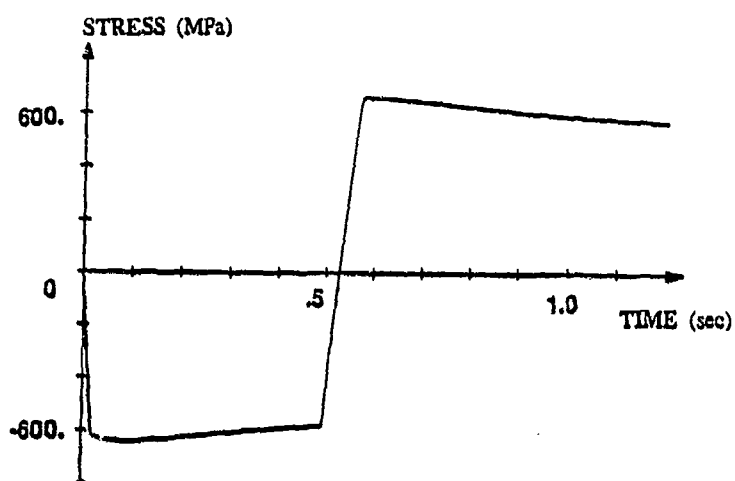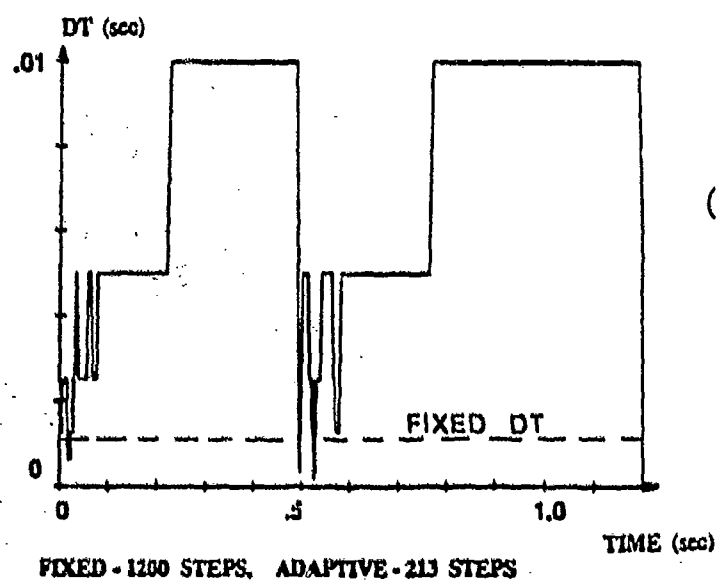
(c) Adaptive time step history

FIXED - 1200 STEPS,   ADAPTIVE - 213 STEPS

Figure 10: Thermo-viscoplastic Response of 1D Model

39
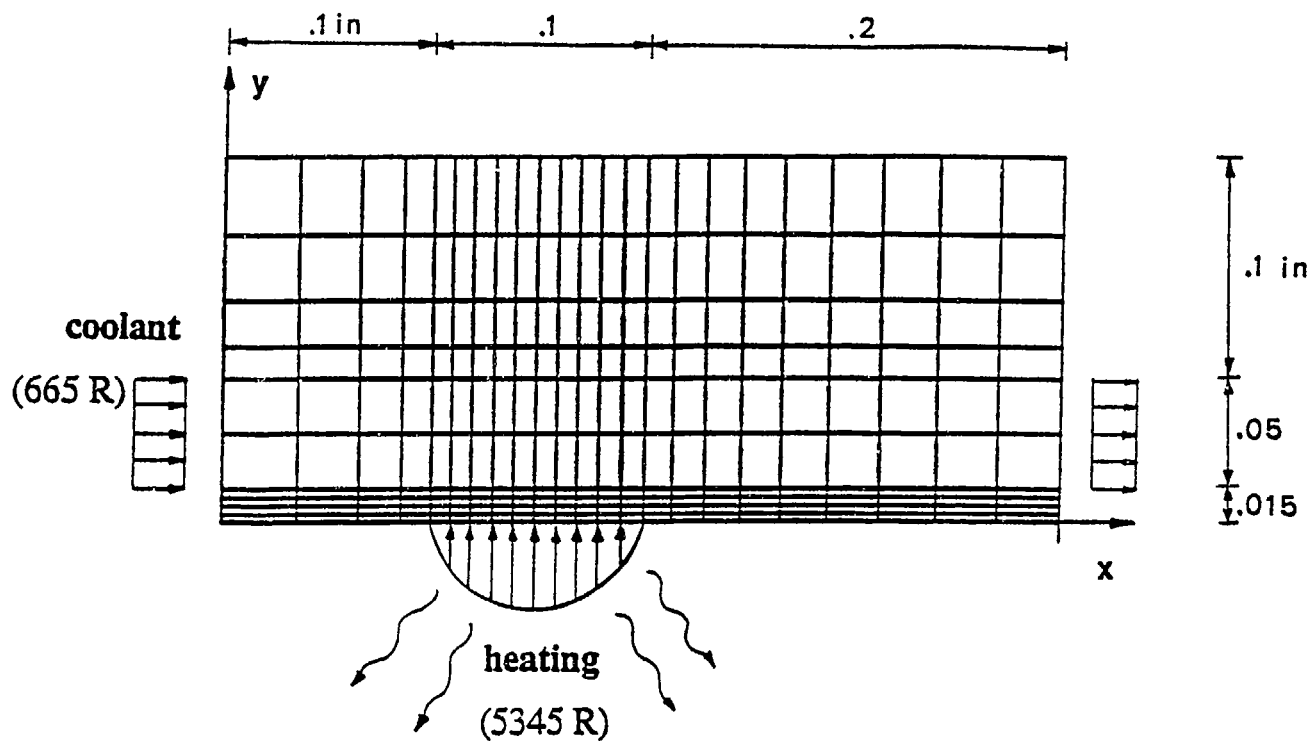
(a) Thermal–structural model
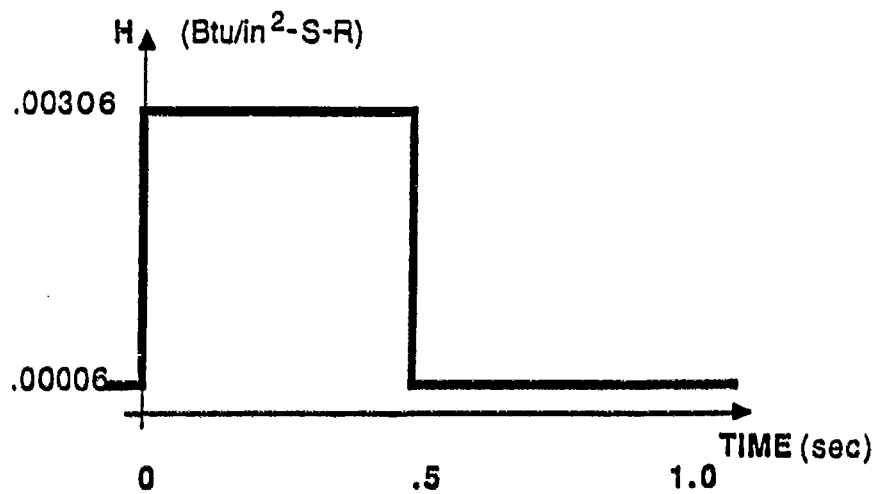
(b) Convection coefficient history

Figure 11: 2D Model of Convectively Cooled Structure

TEMPERATURE (R)

2000.

600.

| 0 | | .5 | | 1.0 | TIME (sec) |
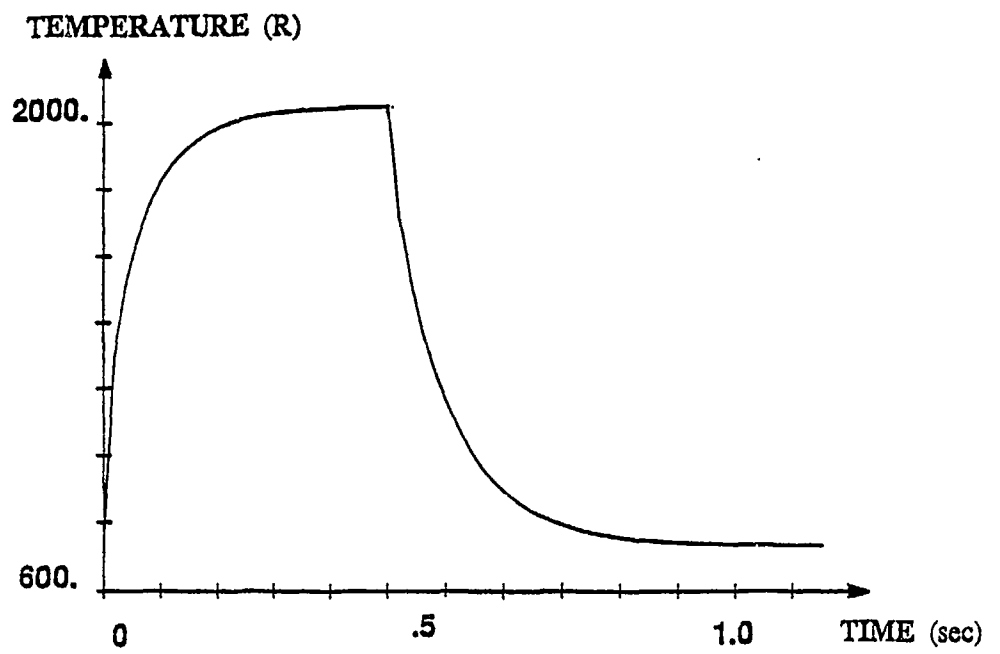
(a) Temperature history at $x = 0.15$ in , $y = 0$
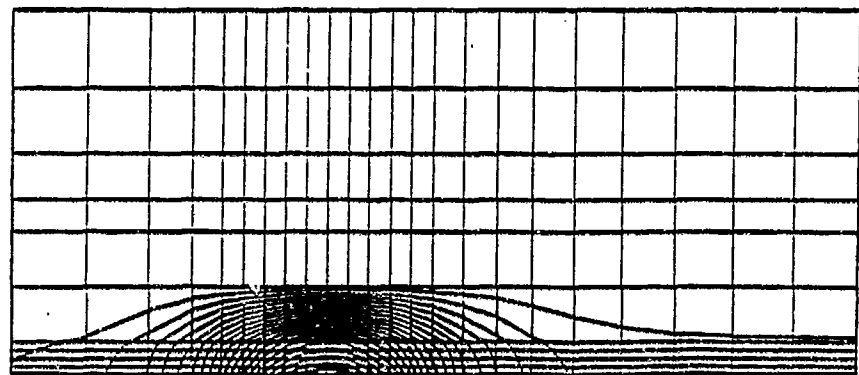
$T_{max} = 2053$ R

(b) Temperature contours at $t = 0.5s$

Figure 12: Thermal Response of 2D Model

41
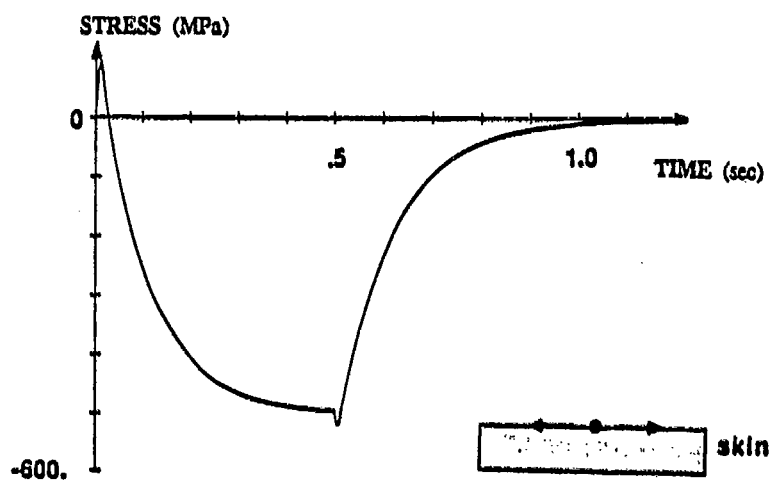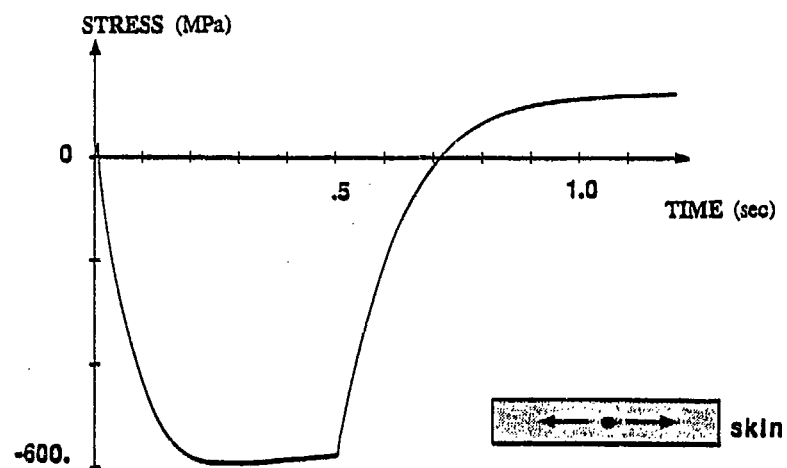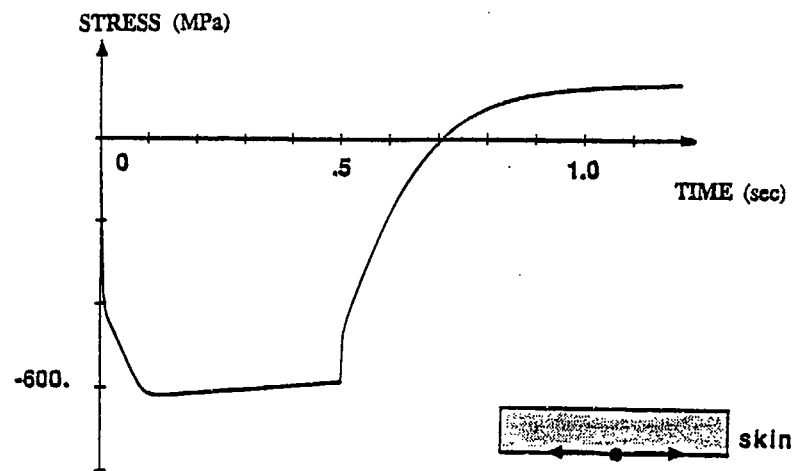
Figure 13: Viscoplastic Stress Histories in Aerodynamic Skin for 2D Model

42
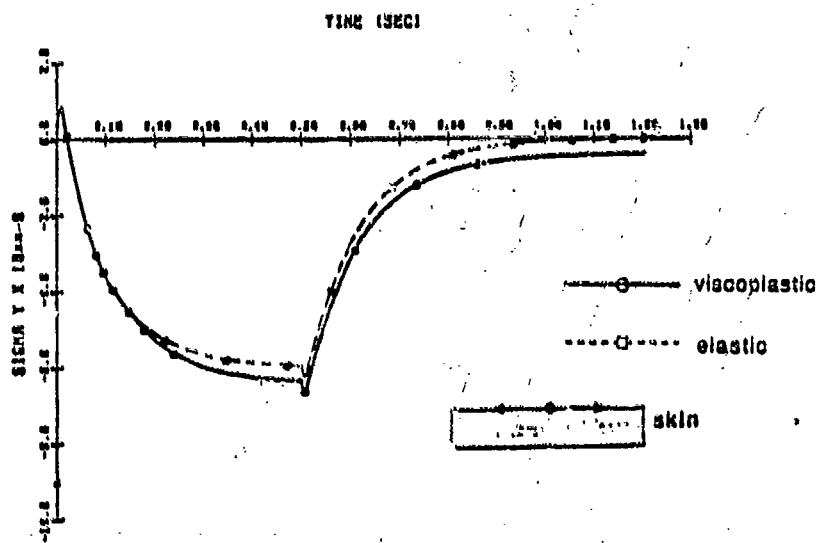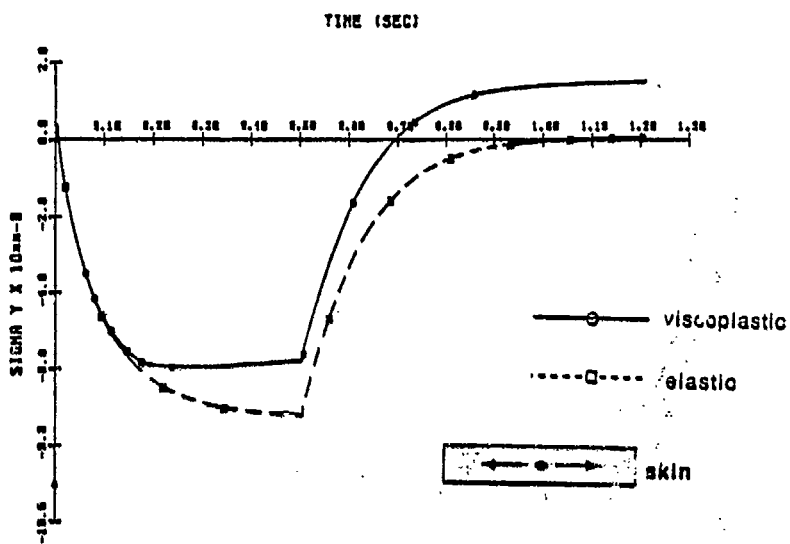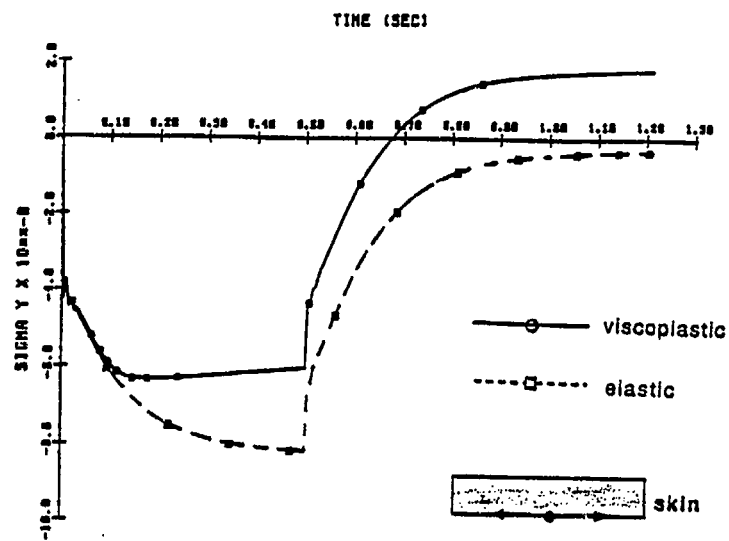
Figure 14: Comparison of Viscoplastic and Elastic Predicted Stress Histories in Aerodynamic Skin

43

STRESS σ_x (MPa)
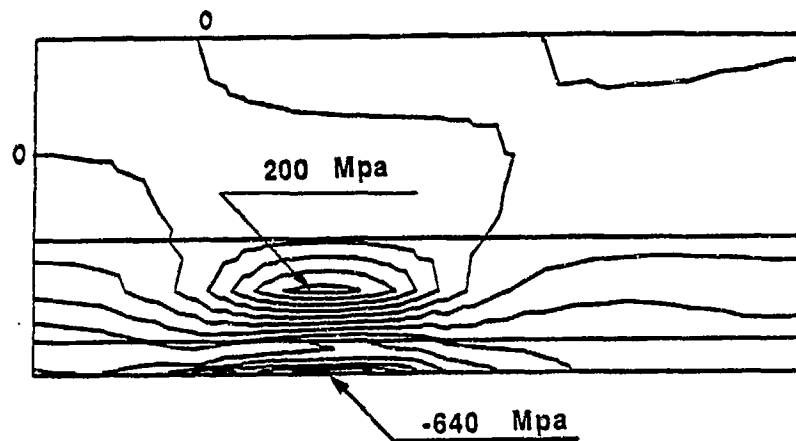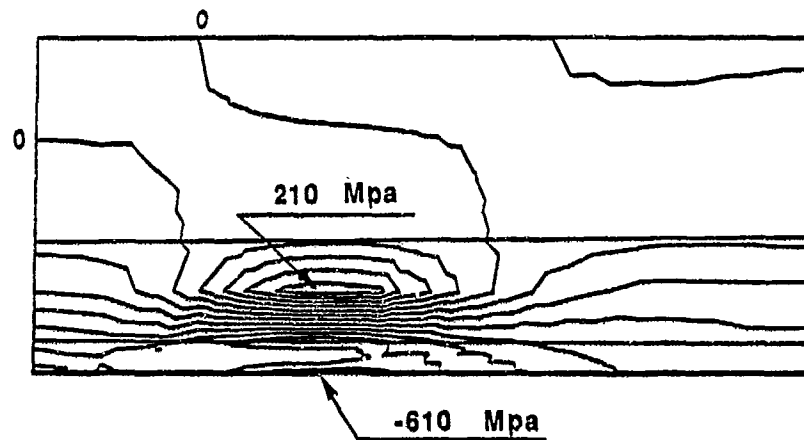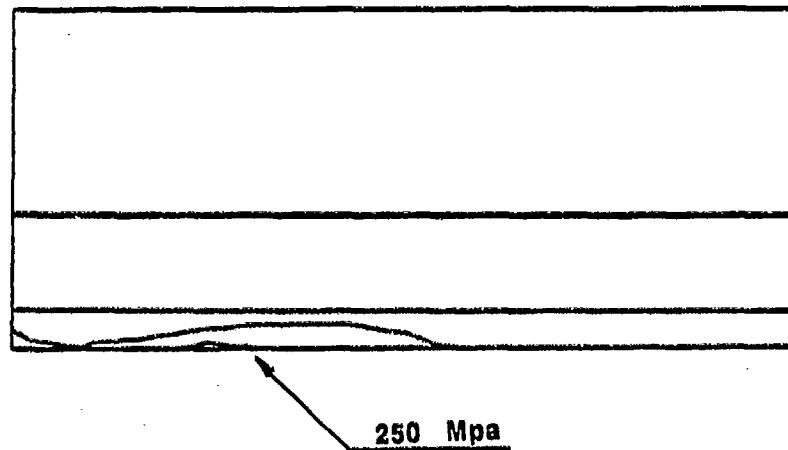
(a) $t = 0.1s$

(b) $t = 0.5s$

(c) $t = 1.0s$

(residual stresses)

Figure 15: Contours of σ_x Stress in 2D Model

44

STRESS σ_y (MPa)
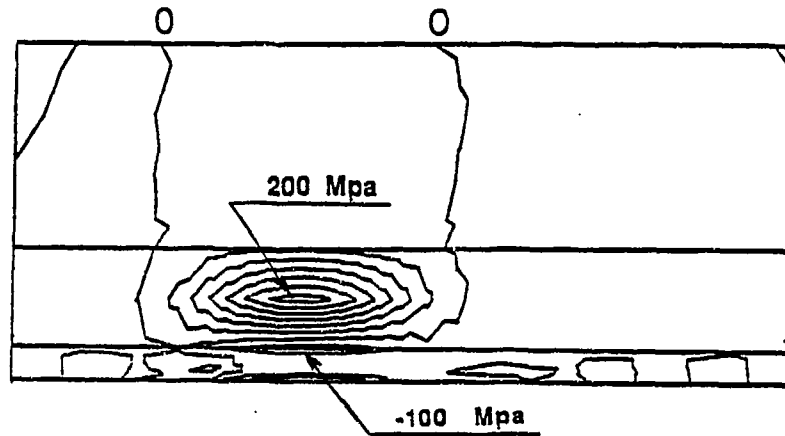
(a) $t = 0.1s$
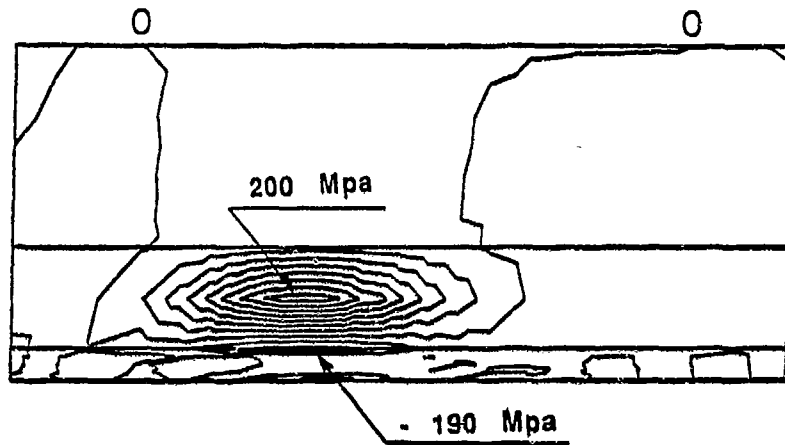
(b) $t = 0.5s$
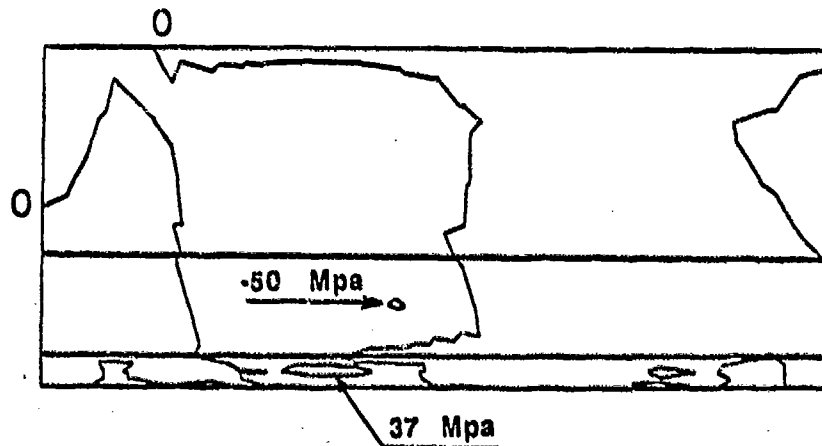
(c) $t = 1.0s$

(residual stresses)

Figure 16: Contours of σ_y Stresses in 2D Model
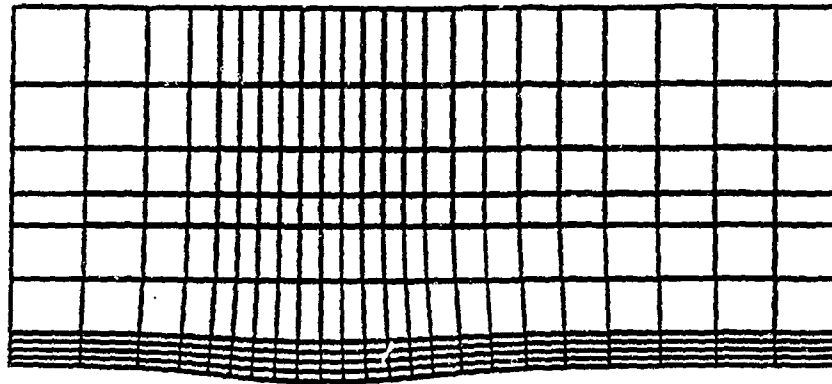
Scale 20×

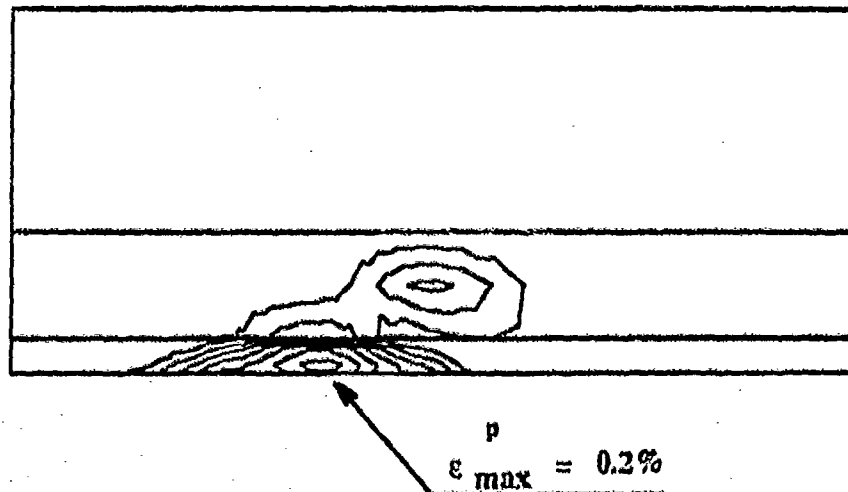$u_{max} = 0.0006$ in

Figure 17: Deformed 2D Model Structure at $t = 0.5s$
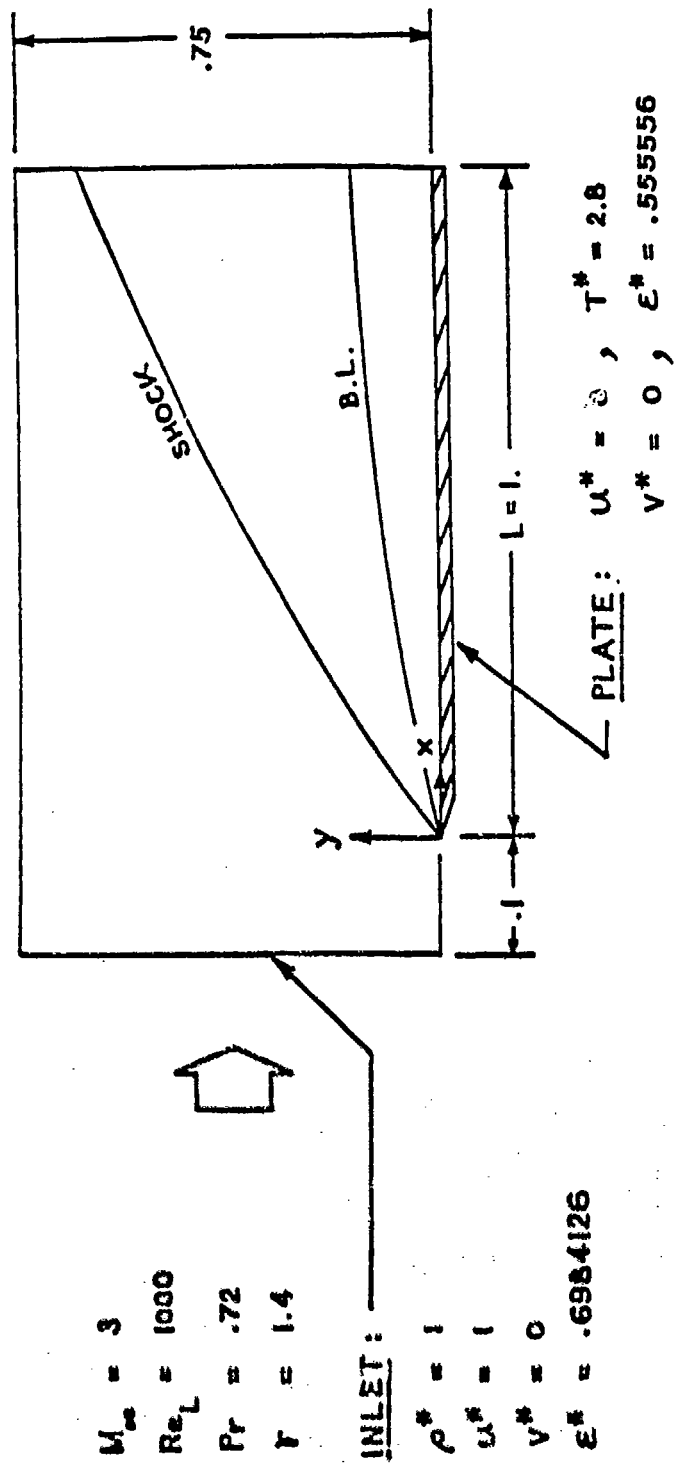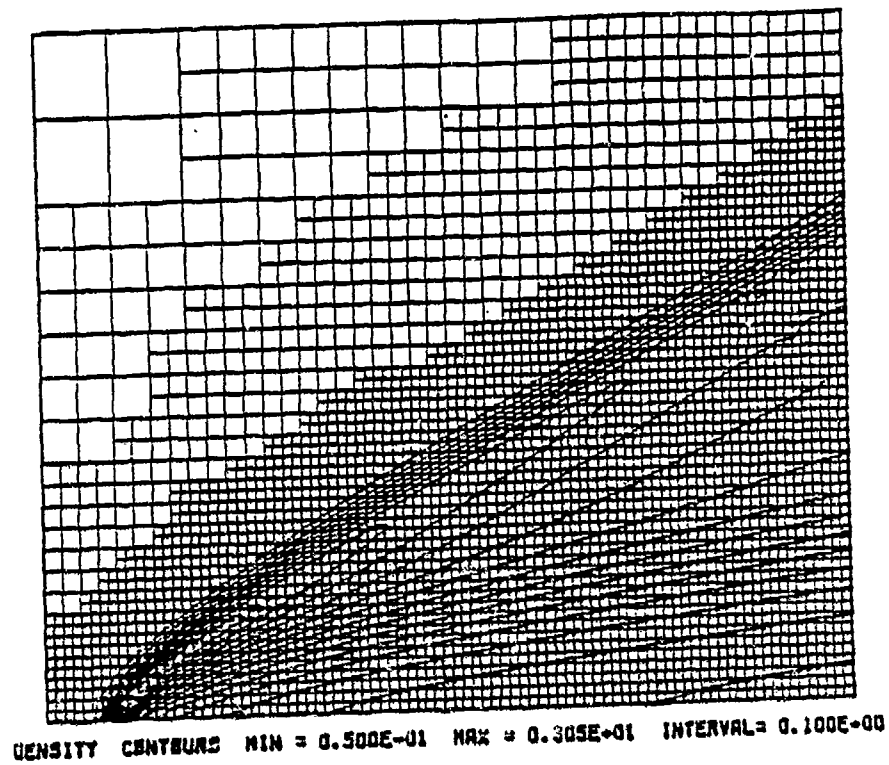

$\varepsilon^{p}_{max} = 0.2\%$

Figure 18: Principal Plastic Strain in 2D Model at $t = .5s$

46

a) Problem Statement

Figure 19: Supersonic Viscous Flow Over Flat Plate (Carter Problem)

DENSITY CONTOURS   MIN = 0.500E-01   MAX = 0.305E+01   INTERVAL= 0.100E+00
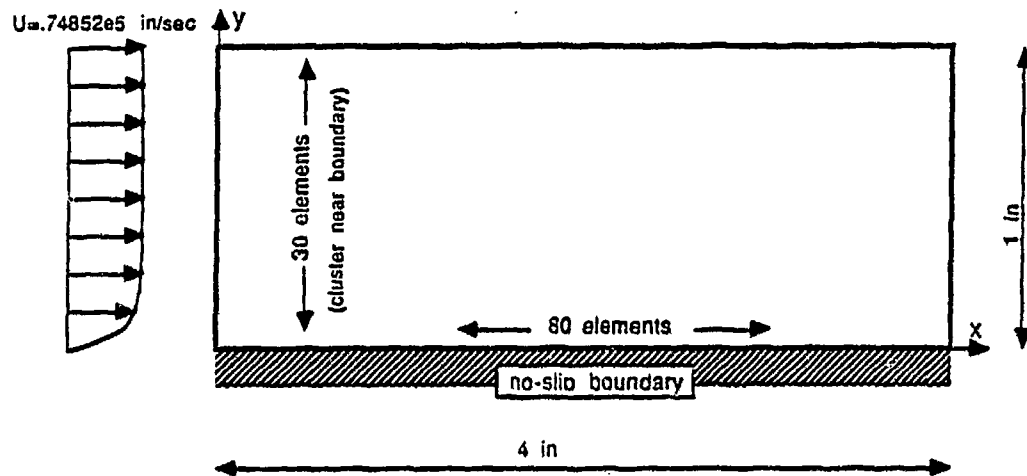
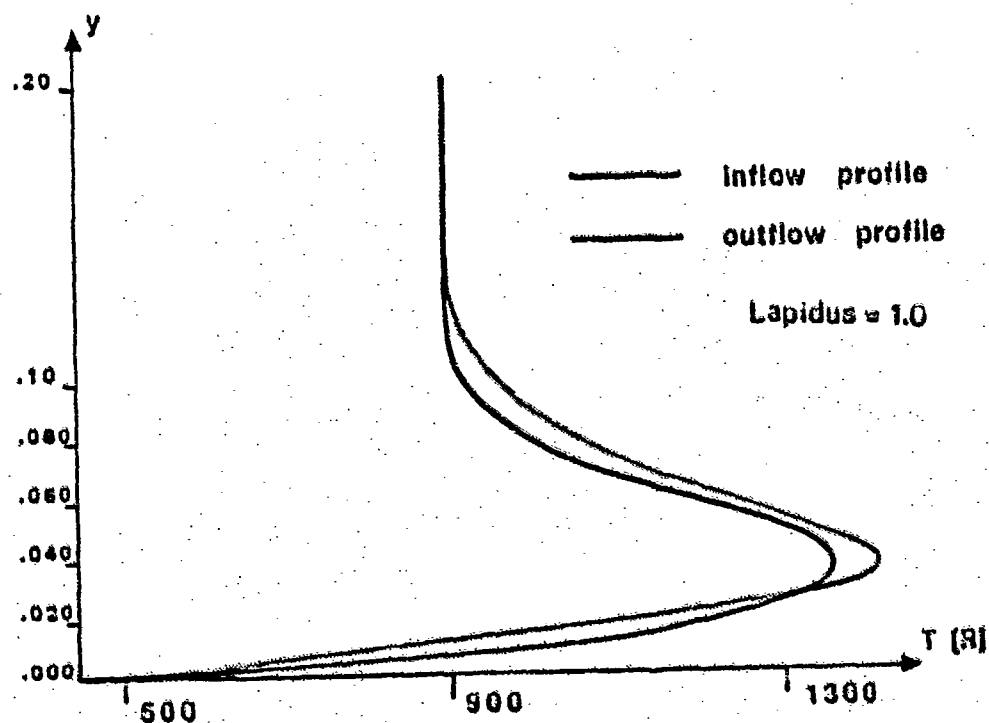(b) Finite element model and density contours
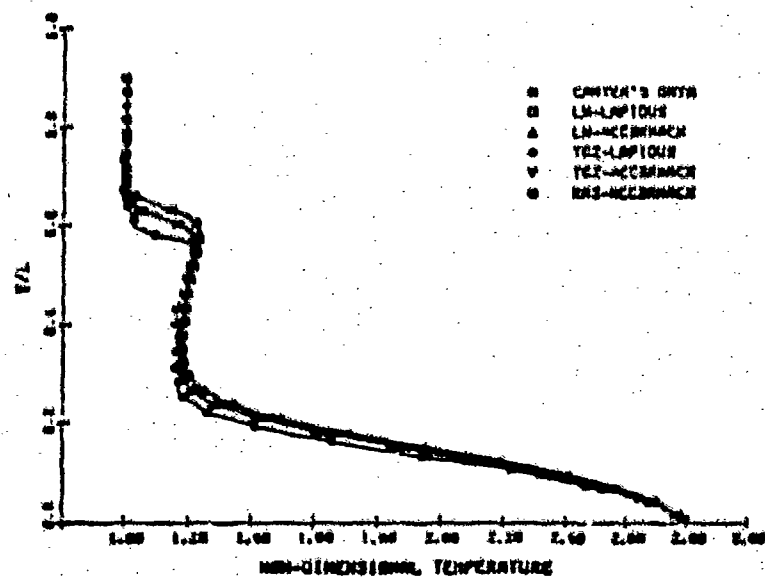
(c) Exit temperature profiles

Figure 10: Supersonic Viscous Flow Over Flat Plate (Carter Problem)

(a) Problem statement

(b) Temperature profiles

Figure 20: Supersonic Boundary Layer

49

Table 1: Data for Thermal Problem

1. Skin and primary structure

$$\rho = 0.283 \ \text{lb}_m / \text{in}^3$$

Temperature Dependent Conductivity and Specific Heat

T [°R]	0	500	1500	3000
K [BTU / in-s-R]	1.23×10^{-4}	1.8×10^{-4}	3.25×10^{-4}	6.0×10^{-4}
Cp [BTU / lb$_m$-R]	0.12	0.135	0.177	0.26

2. Coolant

$$\dot{m} = 7.16 \ 10^{-3} \qquad \text{lb}_m / \text{sec}$$
$$Cp = 3.48 \qquad \text{BTU lb}_m \cdot R$$
$$T_o = 665 \qquad R$$
$$h = 6.2 \times 10^{-3} \qquad \text{BTU} / s \cdot \text{in}^2 \cdot R$$

3. Surface convection

$$T_\infty = 5345 \ R$$
$$h = 6.0 \times 10^{-5} \qquad \text{BTu} / s \cdot \text{in}^2 \cdot R$$

Additional h at time $0 \leq t \leq 0.5$ sec :

$$0 \leq x < 0.1 : \qquad h_{add} = 0$$
$$0.1 \leq x \leq 0.2 : \qquad h_{add} = 3.0 \times 10^{-3} \cos \frac{(x - 0.15)}{0.05} \frac{\Pi}{2} \qquad \text{BTU} / s \cdot \text{in}^2 \cdot R$$
$$0.2 < x \leq 0.4 : \qquad h_{add} = 0$$

4. Surface radiation

$$\sigma = 3.30633 \times 10^{-5} \qquad \text{BTU} / s \cdot \text{in}^2 \cdot R^4$$
$$\varepsilon = 0.8$$
$$\hat{\alpha} = 0.8$$

Table 2: Data for Viscoplastic Analysis

Model Constants for superalloy   B 1900 + Hf

1. Temperature - independent constants

D_o = 1.0 x 10^4 sec $^{-1}$

Z_1 = 3000   MPa

Z_3 = 1150   MPa

r_1 = 2

r_2 = 2

m_1 = 0   MPa^{-1}

m_2 = 0

2. Temperature - Dependent Parameters

T	[°C]	≤ 760	871	982	1093
n		1.055	1.03	0.850	0.70
$Z_2 = Z_o$	[MPa]	2700	2400	1900	1200
A_1	[sec^{-1}]	0	0.0055	0.02	0.25
A_2	[sec^{-1}]	0	0	0	0

3.   Elastic constants

E = 1.987 x 10^5 + 16.78 T - 0.1034 T^2 + 1.143 x 10^{-5} T^3 [MPa]

G = 8.650 x 10^4 - 17.58 + 0.02321 T^2 - 3.464 x 10^{-5} T^3 [MPa]

(with temperature in °C)